Mon. Not. R. Astron. Soc. **296,** 977–994 (1998)

X-ray spectral analysis of elliptical galaxies from *ASCA*: the Fe abundance in a multiphase medium

David A. Buote and A. C. Fabian
Institute of Astronomy, Madingley Road, Cambridge CB3 0HA

Accepted 1998 January 12. Received 1998 January 12; in original form 1997 July 14

ABSTRACT

We present spectral analysis of *ASCA* data of 17 elliptical and three lenticular galaxies most of which have high L_x/L_B. Single-temperature models (MEKAL and Raymond–Smith) give unacceptable fits ($\chi^2_{red} > 1.5$) in most cases and, in agreement with previous studies, give very subsolar abundances, $\langle Z \rangle = 0.19 \pm 0.12\ Z_\odot$ (MEKAL). The spectra for approximately half the sample are fitted better by a cooling-flow model, which in three cases gives a substantially better fit. The abundances derived from the cooling-flow model are also significantly larger, $\langle Z \rangle = 0.6 \pm 0.5\ Z_\odot$. We empirically tested the reliability of the plasma codes in the Fe L region and found no evidence for serious problems with the determined temperatures and abundances.

Two-temperature models give substantially better fits that are formally acceptable ($\chi^2_{red} \sim 1.0$) in all but a few cases. The highest signal-to-noise ratio galaxies (which also have highest L_x/L_B) have fitted temperatures < 2 keV for both components consistent with each being distinct phases of hot gas. The lowest signal-to-noise ratio galaxies (which also have lowest L_x/L_B) generally have a hot component with temperature, $T_H \gtrsim 5$ keV, which is consistent with emission from discrete sources. (We discuss the origin of these two components from analysis of $L_x - L_B$ and L_x/L_B.) The abundances of these two-temperature models are approximately solar, $\langle Z \rangle = 0.9 \pm 0.7\ Z_\odot$ (MEKAL), consistent with a recent multiphase model for the evolution of hot gas in ellipticals. Finally, for several galaxies we find evidence for absorption in excess of the Galactic value and discuss its implications.

Key words: galaxies: elliptical and lenticular, CD – galaxies: evolution – galaxies: general – X-rays: galaxies.

1 INTRODUCTION

The metallicity of the hot X-ray emitting gas in ellipticals is a sensitive diagnostic of their supernova history and thus serves as a powerful discriminant for models of the enrichment of the hot gas (e.g. Loewenstein & Mathews 1991; Ciotti et al. 1991). Previous *ROSAT* and *ASCA* studies have found the metallicities of ellipticals to be very subsolar in contradiction to the standard enrichment models (e.g. Sarazin 1997). This discrepancy has led some authors (Arimoto et al. 1997) to question the reliability of the standard plasma codes, in particular their modeling of the Fe L emission lines.

However, the abundances derived from the plasma codes also depend on the temperature structure of the gas. Because the cooling times are short ($\sim 10^9$ yr) in ellipticals (e.g. Thomas et al. 1986) the hot gas in elliptical galaxies may consist of a continuum of hot and cold phases similar to that expected for galaxy clusters (Nulsen 1986; Thomas, Fabian & Nulsen 1987). Fitting single-temperature models to intrinsically two-temperature spectra can result in a significant underestimate of the metallicity (Buote & Canizares 1994).

Matsumoto et al. (1997) have obtained very subsolar abundances from fitting two-component models to *ASCA* Solid-State Imaging Spectrometer (SIS) and Gas Imaging Spectrometer (GIS) data of a sample of 12 ellipticals, but they restricted the form of the high-temperature component to have the same temperature for each galaxy. That is, Matsumoto et al. combined the data at high energies, $E \sim 4-10$ keV, for the 12 galaxies and found that the composite spectrum is not tightly constrained but equally well described by either a thermal bremsstrahlung model with $T \sim 12$ keV or a power-law model with photon index 1.8. These models, which are thought to describe the emission from discrete sources, are then assumed to be similar for every galaxy and to apply over the full *ASCA* energy band, $E = 0.4-10$ keV. However, these models need not be valid representations for every galaxy, especially for energies below 4 keV where they are only extrapolations.

Hence, there is a need for a study of a larger sample of ellipticals with fewer modelling assumptions. Moreover, the calibration status of *ASCA* has changed significantly over the past year and thus the results of previous studies need to be verified. We have assembled a sample of 20 early-type galaxies (17 E, 3 S0 – see Table 1) with

Table 1. Galaxy properties.

Name	Type	z	B_T^0	$\log_{10} L_B$ erg s^{-1}	σ_0 (km s^{-1})	N_H (10^{21}cm^{-2})	Group
NGC 499	S0$^-$	0.01459	12.64	43.74	237	0.53	LGG 24
NGC 507	LAR0	0.01642	11.76	44.19	366	0.53	LGG 24
NGC 720	E5	0.00572	11.15	43.47	247	0.14	LGG 38
NGC 1332	S0$^-$	0.00508	11.29	43.29	347	0.22	LGG 97
NGC 1399	E1P	0.00483	10.79	43.46	310	0.13	Fornax
NGC 1404	E1	0.00648	11.06	43.35	225	0.13	Fornax
NGC 1407	E0	0.00593	10.93	43.61	285	0.55	LGG 100
NGC 3923	E4-5	0.00556	10.79	43.82	216	0.64	LGG 253
NGC 4374	E1	0.00334	10.23	43.67	287	0.26	Virgo
NGC 4406	E3	-0.00076	10.02	43.76	250	0.26	Virgo
NGC 4472	E2	0.00290	09.32	44.04	287	0.16	Virgo
NGC 4636	E0$^+$	0.00365	10.50	43.58	191	0.17	Virgo
NGC 4649	E2	0.00471	09.83	43.83	341	0.24	Virgo
NGC 5044	E0	0.00898	11.87	43.75	234	0.50	LGG 338
NGC 5846	E0-1	0.00608	11.13	43.77	278	0.42	LGG 393
NGC 6876	SB0$^-$	0.01338	12.45	43.66	231	0.52	LGG 432
NGC 7619	E2	0.01269	12.17	43.79	337	0.50	LGG 473
NGC 7626	E1P	0.01142	12.17	43.70	234	0.50	LGG 473
IC 1459	E3	0.00564	10.96	43.53	308	0.12	LGG 466
IC 4296	E0	0.01255	11.43	44.12	323	0.43	LGG 353

Notes. Morphological types and redshifts are taken from RC3. Total blue magnitudes (B_T^0) and central velocity dispersions (σ_0) are taken from Faber et al. (1989) except for NGC 1332 (Dalle Ore et al. 1991). The luminosities (L_B) corresponding to B_T^0 are computed using the distances from Faber et al. (1989) as reported in Eskridge, Fabbiano & Kim (1995) for $H_0 = 50$ km s^{-1} Mpc^{-1}. Galactic hydrogen column densities (N_H) are from Stark et al. (1992). LGG refers to Garcia (1993).

high L_x/L_B values as listed in Kim, Fabbiano & Trinchieri (1992) to ensure that the X-ray emission is mostly a result of hot gas. These galaxies have archival *ASCA* observations of good quality for most of the sample. We place a premium on the signal-to-noise ratio, S/N, and thus the extraction radii for the spectra are in many cases smaller than in previous studies. This attention to S/N is vital in order to achieve the global χ^2 minima with XSPEC for our models with many fitting parameters. We fit as many temperature components as are demanded by the data to achieve a good fit without any restrictions on the temperatures. We also examine the reliability of the plasma codes in the Fe L spectral band directly from the sample.

The organization of the paper is as follows. In Section 2 we describe the details of the observations and data analysis. The results of the single-temperature fits and the empirical test of the plasma codes are given in Section 3.1. We discuss the two-temperature (and three-temperature) fits in Section 3.2. In Section 4 we discuss the evidence and implications for excess absorption in several of the galaxies. Finally, we summarize and give our conclusions in Section 5 .

2 OBSERVATIONS AND DATA REDUCTION

The *ASCA* satellite (Tanaka, Inoue & Holt 1994) consists of four detectors each illuminated by a dedicated X-ray telescope. Two of the detectors are X-ray CCD cameras (Solid-State Imaging Spectrometers – SIS0 and SIS1) and two are proportional counters (Gas Imaging Spectrometers – GIS2 and GIS3). Since the X-ray luminosity of the early-type galaxies in our sample is thought to be dominated by thermal emission with $T \sim 1$ keV[1] (Forman, Jones & Tucker 1985; Canizares, Fabbiano & Trinchieri 1987; Kim et al. 1992), and the effective area and energy resolution of the SIS is substantially greater than that of the GIS for energies $\sim$0.5−1.5 keV (see Table 2), the SIS data has far better S/N over the important energies for constraining spectral models and for probing the Fe L emission region.

That is, the fluxes of bright early-type galaxies above 2 keV are typically $\lesssim$10 per cent of the 0.5−2 keV fluxes (e.g. Table 7, later) which indicates that even though the effective areas of the SIS and GIS are comparable for energies $\sim$2−5 keV (the SIS being slightly *better* on average) the important constraints on spectral models fitted over $\sim$0.5−5 keV are determined almost completely by the SIS data because of its substantial advantage in effective area for energies below 2 keV and its superior energy resolution over the entire *ASCA* band (e.g. Buote & Canizares 1997). Since the SIS data dominates the constraints on spectral models of early-type galaxies, any small differences in the model parameters obtained from jointly

Table 2. SIS versus GIS.

Energy (keV)	Area (cm^2) SIS	GIS	ΔE (eV) SIS	GIS
0.75	60	6	70	∼200
1.00	140	50	75	∼200
1.25	175	100	80	225
1.50	200	130	85	240
2.00	150	160	90	250
5.00	130	120	150	400

Comparison of the effective area and energy resolution of the SIS and the GIS. These values are approximate as they were obtained from visual inspection of figs 8.4a, 8.4b, and 9.5 of the *ASCA* Technical Description (Appendix E, AN 97-OSS-02). The spectral resolution of the SIS refers to 1994 February.

[1]Throughout the paper we set $k_B T \rightarrow T$.

Table 3. *ASCA* SIS observation properties.

Name	Sequence #	Exposure (10^3s)		Count Rate (10^{-2} ct s^{-1})		R (arcmin)		R (kpc)	
		SIS0	SIS1	SIS0	SIS1	SIS0	SIS1	SIS0	SIS1
NGC 499	61007000	25.3	25.6	7.5	7.0	2.9	2.8	74.7	72.2
	63026000	34.9	33.7	11.6	9.1	3.6	3.4	92.8	87.6
NGC 507	61007000	25.3		22.0		4.2		121.3	
NGC 720	60004000	30.2	32.0	2.5	1.4	2.5	2.0	23.7	19.0
NGC 1332	63022000	53.6	53.1	1.8	1.0	2.7	2.1	22.3	17.3
NGC 1399	80038000	14.9	10.3	34.4	33.8	4.9	4.4	38.9	34.8
	80039000	14.5	13.1	36.2	13.9	4.6	3.2	36.3	25.3
NGC 1404	80038000	14.9	10.3	8.2	8.9	2.7	2.3	21.4	18.2
	80039000	14.5	13.1	8.0	4.0	2.5	2.0	19.8	15.8
NGC 1407	63021000	31.7	31.3	4.7	3.7	3.0	2.7	30.3	27.3
NGC 3923	82016000	20.5	12.7	1.7	1.3	2.0	2.0	24.1	24.1
NGC 4374	60007000	13.5	12.7	4.0	4.4	2.0	2.0	15.7	15.7
NGC 4406	60006000 (4ccd)	11.0	9.1	38.0	26.2	5.5	5.0	43.2	39.3
	60006000 (2ccd)	5.3	5.2	36.2	20.3	5.3	4.6	41.6	36.1
NGC 4472	60029000	16.3	12.5	36.2	25.7	4.1	3.5	32.2	27.5
	60030000	17.0	13.2	32.3	20.8	4.3	2.4	33.8	18.8
NGC 4636	60032000	33.2	24.8	40.6	27.6	5.0	4.6	39.3	36.1
NGC 4649	60006000 (2ccd)	16.7		13.9		3.0		23.6	
	61005000 (4ccd)	19.2		13.8		3.0		23.6	
NGC 5044	80026000 + 80026010	16.3	12.2	117.4	78.4	5.5	5.1	100.0	92.3
NGC 5846	61012000	30.3	16.7	19.9	11.5	4.0	3.5	53.3	46.6
NGC 6876	81020000	18.6		2.5		2.0		53.4	
NGC 7619	63017000	52.5	48.5	4.7	3.4	3.0	3.0	54.5	54.5
NGC 7626	63017000	52.5	48.5	0.9	1.1	2.0	2.0	36.3	36.3
IC 1459	60005000	23.8	17.4	3.9	1.7	2.5	2.0	23.3	18.7
IC 4296	61006000	32.9	31.3	4.7	2.7	3.1	2.6	70.7	59.3

Notes. The exposures include any time filtering. The count rates are background subtracted within the circle of radius R. For NGC 4406 we give the half-diagonal of the rectangular regions. Aperture radii in kpc are computed using the distances from Faber et al. (1989) as reported in Eskridge, Fabbiano & Kim (1995) for $H_0 = 50\,\mathrm{km\,s^{-1}\,Mpc^{-1}}$.

fitting SIS and GIS data of early-type galaxies may be because of mismatches in calibration between the two instruments; e.g. the gain calibration of the GIS (Idesawa et al. 1997). Hence, we focus on the SIS data, although throughout the paper we illustrate pertinent results using the GIS data for representative galaxies. The reduction of the SIS and GIS data was performed using the standard XSELECT, FTOOLS, and IRAF-PROS software.

We list details of the observations in Table 3. Because the SIS0 and SIS1 (and GIS2 and GIS3) have different energy responses and gains their data must be fitted separately. The same applies for different observations of the same galaxy since the energy response and gain vary significantly with time. As a result, for a galaxy with multiple observations, if one of the sequences has a substantially smaller exposure time than the others, it will not contribute significantly to the spectral fits. (And any residual differences caused by incorporating the lower S/N observation may just be systematics owing to background subtraction or calibration.) Moreover, the aperture size used to extract the spectrum for the lower S/N sequence will be necessarily smaller than the others, which could lead to inconsistencies. (We describe our determination of aperture sizes below.) Hence, for a few galaxies with multiple observations (NGC 507, 4374 and 5044) we ignored these sequences with much worse S/N.

Similarly, for a given observation the SIS0 data has higher S/N than the SIS1 data because the screening criteria for events is much more severe for the SIS1. If a great disparity in S/N existed between the two detectors then we analysed only the high S/N observation (NGC 4649 and 6876). For NGC 507 we excluded the SIS1 data because of anomalies that we discuss in Section 3.

For each galaxy we analyzed the data generated by the standard processing software that were filtered with the default screening criteria (see The *ASCA* Data Reduction Guide 1997). We further screened the data by excluding time intervals of high background from analysis of the light curves. For NGC 720 and 1332 we used the events screened according to the criteria in Buote & Canizares (1997) modified by the light-curve analysis.

The final filtered events were then extracted from a circular region positioned by eye on the galaxy centre. A circular region was chosen because the standard software which incorporates information on effective area and corrects the spectra for vignetting (i.e. FTOOLS task ASCAARF) currently performs best on circular regions. However, for NGC 4406 we used a square region because the X-ray emission is highly asymmetrical which offsets the benefits of a circular region in ASCAARF.

Our guiding principle for choosing the radius of the circle for a particular galaxy was to maximize the S/N of the background-subtracted counts within the $\sim$0.5$-$5 keV energy band. We modified the S/N criterion according to other considerations. We tried to limit as much as possible the circular aperture to a single CCD because the responses vary from chip to chip. (For the cases where the source counts extended over more than one chip we followed the standard procedure and averaged the response matrices according to the number of source counts on each chip. The gaps between chips were excluded.) For the galaxies having a nearby bright

source (e.g. NGC 1399 and 1404; NGC 499 and 507) we chose a higher S/N cut-off to reduce contamination from the other source.

The background for each galaxy was chosen from source-free regions of the CCDs. Although it is preferred to take the background from the same region of the CCDs as the source in order to insure the same vignetting correction (i.e. using a background determined from a deep exposure of a blank field), the variations of the local background due to environment and peculiarities for a particular observation (e.g. contamination from the bright Earth, the Sun, the South Atlantic Anomaly) outweigh the vignetting consideration for the SIS. However, since the background increases markedly with distance from the centre of the field of the GIS (Ishisaki et al. 1997), we used the blank fields for the background estimates of the GIS data. In any event, the results using a local background generally differ unimportantly from those when a background template constructed from a deep observation of a blank field is used (e.g. Buote & Canizares 1997).[2]

Finally, the source and background spectra for each galaxy were extracted in 512 pulse invariant (PI) bins after correcting for temporal SIS gain variations and the degradation owing to charge-transfer inefficiency. We mention that we made the required corrections to fix problems in the response matrices generated by the standard reduction software as described on the *ASCA* Guest Observer Facility WWW pages (as of 1997 May). Also, the GIS background templates were rise-time filtered (i.e. with FTOOL GISCLEAN) to match the screening of the galaxy observations.

3 SPECTRAL FITTING

It has been known since the operation of the *Einstein Observatory* that the X-ray emission of early-type galaxies mostly originates from a hot interstellar medium (Forman et al. 1979), with an additional contribution from the integrated emission from X-ray binaries which are most important for the galaxies with the smallest ratios of X-ray to blue-band optical luminosity (Canizares et al. 1987). The results from the performance-verification phase of *ASCA* showed that the brightest ellipticals in X-rays have emission lines consistent with those originating from a thin hot thermal plasma (Awaki et al. 1994). The form of the spectrum arising from discrete sources is not well constrained, but is consistent with a high-temperature $T \gtrsim 5$ keV thin thermal plasma (Kim et al. 1992; Matsumoto et al. 1997).

Hence, we concentrate on thin thermal models modified by photoelectric absorption arising from the ISM of our galaxy. We allow for the possibility of intrinsic absorption as seen in galaxy clusters (White et al. 1991) if the fit to the galaxy spectrum is significantly improved. Since the hot gas need not be in a single phase and the X-ray emission may contain a significant contribution from discrete sources, we fit as many absorbed temperature components as are required by the *ASCA* data. [As stated in Section 1, we do not assume the presence of a discrete (or other hard) component with a predetermined functional form for all galaxies.]

To model the emission of a thin thermal plasma we primarily use the MEKAL code which is a modification of the original MEKA code (Mewe, Gronenschild, & van den Oord 1985; Kaastra & Mewe 1993) where the Fe L shell transitions crucial to the X-ray emission of ellipticals have been re-calculated (Liedahl, Osterheld & Goldstein 1997). We take solar abundances according to Anders & Grevesse (1989) and photoelectric absorption cross sections according to Balucińska-Church & McCammon (1992). Although not as accurate as the MEKAL model we also employ the Raymond–Smith code (Raymond & Smith 1977) since it has been used in most previous studies.

We also consider a cooling-flow model based on the MEKAL code where the gas cools continuously from some upper temperature, $T_{\rm max}$. The emissivity of the cooling gas is described in Johnstone et al. (1992). Although this model may be more appropriate for the cores of galaxy clusters since it does not include potential heat sources which may be important in galaxies, it provides a simple and convenient exploration of the effects of cooling-flow spectra on the *ASCA* galaxy data. The cooling-flow spectrum assumes that the gas cools at constant pressure. The pressure itself does not enter into the calculation, and the same spectrum results from different parcels of gas cooling at different pressures. Provided that the gas at different radii (and thus different pressures) starts from the same temperature and cools before flowing a significant distance, it is therefore a good approximation. In practice, gravitational work will be carried out as the gas flows, so the true result will be more complicated (in a manner which depends on the degree of flow). An additional temperature component is the simplest modification that can be made for this effect (see Section 3.2.3).

All of the spectral fitting was implemented with the software package XSPEC (Arnaud 1996) using the χ^2 minimization method. In order for the weights to be valid for the χ^2 method we regrouped the PI bins such that each group contained at least 20 counts. We restricted the fits to energies above 0.5 keV ($\sim$0.55 keV) because of uncertainties in the SIS response at lower energies. We also exclude energies > 5 keV because the S/N of the bins at these energies is generally too low to significantly affect the fits and these energies tend to be dominated by uncertainties in the background level of the SIS and to calibration errors (Gendreau & Yaqoob 1997). The normalizations of the SIS0 and SIS1 are fitted separately as are the normalization of multiple observations of the same galaxy. (For the GIS data we analysed energies $0.8 - 9$ keV.)

For NGC 507 we found that the spectral shapes of the SIS0 and SIS1 differed substantially. However, we find no such discrepancy for the NGC 499 data taken from the NGC 507 observation. (The N499 and N507 data are take from different chips of the SIS.) We compared the NGC 507 data with those from a lower S/N observation (61007010) and found that the SIS0 spectra are consistent. (The SIS1 data for 61007010 have too low S/N to make a useful comparison.) The GIS data give fitted temperatures and abundances and reduced χ^2 in excellent agreement with the SIS0 data. Thus we restrict our analysis of NGC 507 to the SIS0 data. (We mention that we find no similar SIS0/SIS1 discrepancy for the remaining 19 galaxies.)

3.1 Single-component fits

3.1.1 Results

In Table 4 we list the results of simultaneously fitting a single absorbed MEKAL model to the available SIS0 and SIS1 spectra of each galaxy listed in Table 3. In Fig. 1 we show the spectral fits of NGC 1332 and 4649 (among the best S/N for the lowest $L_{\rm x}/L_{\rm B}$) and NGC 4472 and 5044 (among the best S/N for the highest $L_{\rm x}/L_{\rm B}$). (For those galaxies with multiple observations we show the observation with the longest exposure.) In almost all cases the fits are formally quite poor with reduced $\chi^2 > 1.5$. For the X-ray brightest galaxies (and those with largest $L_{\rm x}/L_{\rm B}$) the residuals of the fits tend

[2]Typically the fluxes show the largest differences between the blank sky templates and a local background. The fitted temperatures and abundances are mostly unaffected.

Table 4. Single-temperature fits.

Name	Model	$N_{\rm H}$ (10^{21} cm^{-2})	T (keV)	Z ($Z_\odot$)	$\dot{M}_{\rm gas}$ $M_\odot$ yr^{-1}	$\Delta\chi^2(N_{\rm H})$	χ^2	dof	$\chi^2_{\rm red}$
NGC 499	MEKAL	2.0	0.67	0.31		49.4	323.3	205	1.58
	CF	2.4	0.96	0.48	45.9	122.0	334.6	205	1.63
NGC 507	MEKAL	$1.2^{+0.3}_{-0.4}$	$1.27^{+0.06}_{-0.06}$	$0.38^{+0.10}_{-0.08}$		12.3	68.4	74	0.92
	CF	$3.0^{+0.5}_{-0.6}$	$2.16^{+0.27}_{-0.20}$	1.9(> 1.3)	$34.5^{+8.3}_{-7.7}$	96.1	80.2	74	1.08
NGC 720	MEKAL	...	0.63	0.08		...	94.2	48	1.96
	CF	...	1.11	0.12	0.94	...	90.9	48	1.89
NGC 1332	MEKAL	...	0.65	0.06		...	173.6	66	2.63
	CF	...	1.17	0.08	0.49	...	169.1	66	2.56
NGC 1399	MEKAL	0.6	1.27	0.37		29.9	435.8	256	1.70
	CF	$1.8^{+0.3}_{-0.2}$	$2.5^{+0.2}_{-0.1}$	(> 1.7)	$1.14^{+0.13}_{-0.12}$	233.7	341.3	256	1.33
NGC 1404	MEKAL	1.4	0.56	0.27		20.6	196.6	127	1.55
	CF	2.1	0.73	0.44	13.9	39.6	197.5	127	1.55
NGC 1407	MEKAL	...	0.92	0.10		...	166.4	94	1.77
	CF	...	$2.4^{+0.3}_{-0.2}$	$0.38^{+0.14}_{-0.11}$	$0.63^{+0.09}_{-0.10}$	...	138.4	94	1.47
NGC 3923	MEKAL	...	0.64	0.07		...	48.3	23	2.10
	CF	...	1.13	0.11	0.84	...	45.3	23	1.97
NGC 4374	MEKAL	...	$0.70^{+0.05}_{-0.04}$	$0.09^{+0.04}_{-0.03}$		...	72.2	52	1.39
	CF	...	$1.17^{+0.16}_{-0.13}$	$0.13^{+0.08}_{-0.04}$	$0.55^{+0.15}_{-0.13}$	...	74.7	52	1.44
NGC 4406	MEKAL	$1.2^{-0.3}_{+0.4}$	$0.73^{+0.03}_{-0.02}$	$0.27^{+0.06}_{-0.04}$		23.4	223.5	188	1.19
	CF	$2.3^{+0.4}_{-0.3}$	$1.03^{+0.07}_{-0.06}$	$0.69^{+0.34}_{-0.20}$	$4.7^{+1.0}_{-0.8}$	116.1	213.6	188	1.14
NGC 4472	MEKAL	0.8	0.97	0.26		53.6	495.4	240	2.06
	CF	$2.2^{+0.1}_{-0.3}$	$1.59^{+0.06}_{-0.06}$	$1.31^{+0.31}_{-0.23}$	$1.94^{+0.19}_{-0.18}$	338.5	301.1	240	1.26
NGC 4636	MEKAL	1.2	0.66	0.28		86.9	280.6	138	2.03
	CF	1.9	0.91	0.48	5.61	245.7	295.3	138	2.14
NGC 4649	MEKAL	1.6	0.83	0.20		51.3	210.1	99	2.12
	CF	2.3	1.39	0.56	1.37	99.8	179.7	99	1.82
NGC 5044	MEKAL	0.9	0.95	0.25		30.8	443.9	161	2.76
	CF	$2.5^{+0.2}_{-0.2}$	$1.42^{+0.05}_{-0.04}$	$1.03^{+0.17}_{-0.15}$	$75.7^{+6.8}_{-6.5}$	542.5	228.5	161	1.42
NGC 5846	MEKAL	$1.7^{+0.6}_{-0.4}$	$0.67^{+0.04}_{-0.03}$	$0.21^{+0.06}_{-0.04}$		29.5	139.9	107	1.31
	CF	$2.0^{+0.4}_{-0.4}$	$1.02^{+0.10}_{-0.06}$	$0.38^{+0.09}_{-0.08}$	$9.4^{+3.0}_{-2.3}$	51.1	109.4	107	1.02
NGC 6876	MEKAL	2^{+4}_{-1}	$0.88^{+0.15}_{-0.25}$	$0.14^{+0.57}_{-0.07}$		3.3	22.6	17	1.33
	CF	$3.1^{+2.8}_{-1.7}$	$1.3^{+0.6}_{-0.4}$	$0.3^{+1.1}_{-0.2}$	$8.8^{+21}_{-5.5}$	8.1	20.5	17	1.20
NGC 7619	MEKAL	$3.1^{+0.9}_{-0.9}$	$0.69^{+0.5}_{-0.5}$	$0.31^{+0.23}_{-0.10}$		44.4	117.3	98	1.20
	CF	$3.3^{+0.5}_{-0.8}$	$1.03^{+0.14}_{-0.10}$	$0.46^{+0.25}_{-0.13}$	$17.5^{+6.2}_{-5.8}$	70.4	112.1	98	1.14
NGC 7626	MEKAL	...	0.88	0.08		...	85.6	52	1.65
	CF	...	$2.31^{+0.54}_{-0.44}$	$0.38^{+0.39}_{-0.19}$	$0.72^{+0.26}_{-0.19}$	...	70.2	52	1.35
IC 1459	MEKAL	...	2.69	0.00		...	100.3	55	1.82
	CF	...	$7.4^{+3.0}_{-1.7}$	$0.11^{+0.13}_{-0.06}$	$0.14^{+0.04}_{-0.04}$	...	83.5	55	1.52
IC 4296	MEKAL	...	1.02	0.08		...	203.2	91	2.23
	CF	...	$3.3^{+0.7}_{-0.5}$	$0.47^{+0.20}_{-0.16}$	$1.83^{+0.37}_{-0.36}$	...	137.0	91	1.49

Notes. Results of fitting either one MEKAL model or a cooling-flow model each modified by photoelectric absorption. If allowing $N_{\rm H}$ to be free significantly improved the fit, we give the best-fitting value of $N_{\rm H}$ and the change in χ^2 denoted by $\Delta\chi^2(N_{\rm H})$. Otherwise '...' denote that $N_{\rm H}$ is kept at its Galactic value. For fits where $\chi^2 < 1.5$ we also list 90 per cent confidence limits on one interesting parameter. The gas mass deposition rates, $\dot{M}_{\rm gas}$, are quoted in the 0.5–5 keV band for the SIS0. For galaxies with multiple observations, the highest S/N observation is typically quoted.

to be most pronounced around 1 keV, whereas the fainter galaxies (and those with smallest $L_{\rm x}/L_{\rm B}$) tend to show the largest significant residuals at higher energies, $E \gtrsim 3$ keV.

The temperatures and abundances determined from the single-temperature fits are qualitatively consistent with previous *ASCA* studies of the ellipticals in our sample (Awaki et al. 1994; Matsushita et al. 1994; Loewenstein et al. 1994; Fukazawa et al. 1996; Buote & Canizares 1997; Arimoto et al. 1997; Matsumoto et al. 1997; Iwasawa, White, & Fabian 1997) modulo expected small systematic differences as a result of different source region sizes, background region definitions, thermal emission codes used, current status of SIS calibration etc. In particular, our single-temperature models reproduce the extremely subsolar abundances found in the above studies. All the galaxies have best-fit $Z < 0.4\,Z_\odot$ and most have $Z \lesssim 0.15\,Z_\odot$. The mean abundance and standard deviation are $\langle Z\rangle = 0.19 \pm 0.12\ Z_\odot$.

For half of the galaxies in our sample the fits improved significantly if $N_{\rm H}$ was allowed to be a free parameter. This improvement affects only the energy bins for $E \sim 0.5 - 1.0$ keV. In each of these cases, significant excess absorption above the Galactic value is indicated. The excess absorption we find for these galaxies agrees qualitatively with those determined from the previous *ASCA* studies listed above. However, with *ROSAT* only NGC 1399 showed evidence for excess absorption (Rangarajan et al. 1995) while several of the galaxies which we find to require excess absorption were not found to require it with *ROSAT*: NGC 499 and 507 (Kim & Fabbiano 1995), NGC 4472 (Forman et al. 1993; Irwin & Sarazin 1996), NGC 4636 (Trinchieri et al. 1994), NGC 4649 and 7619

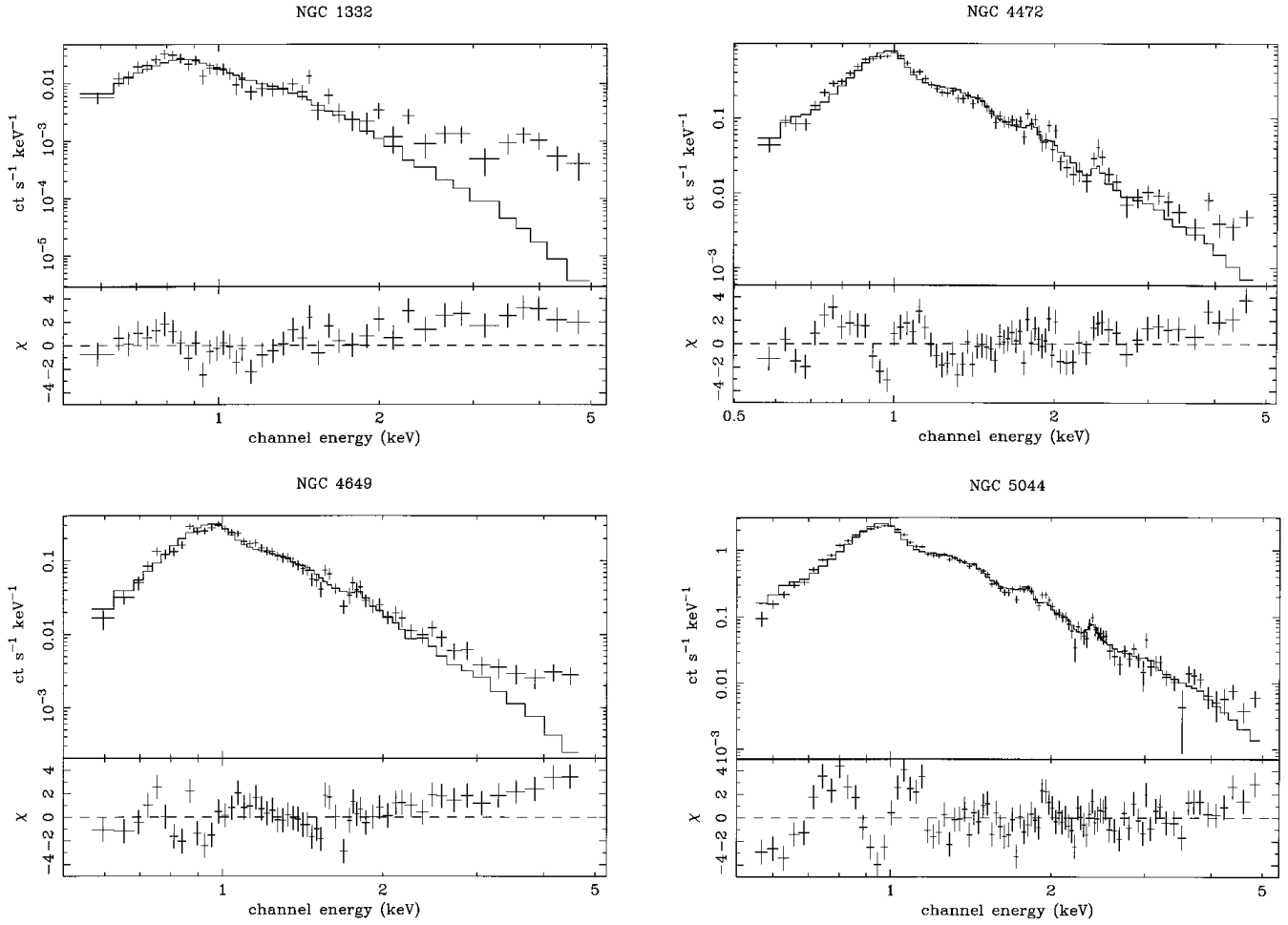

Figure 1. Absorbed single-temperature (MEKAL) fits to the spectra of NGC 1332, NGC 4472, NGC 5044 and NGC 4649. Only the SIS0 data is shown.

(Trinchieri, Fabbiano & Kim 1996), NGC 5044 (David et al. 1994), and several others (Davis & White 1996). We discuss in detail the evidence and implications for this excess absorption in Section 4.

In terms of both χ^2 and the fitted parameters the Raymond–Smith model gives broadly comparable results to the MEKAL model when fitted over the $\sim$0.5–5 keV range. (In agreement with many previous studies we find that the Raymond–Smith model tends to give higher temperatures and smaller abundances than the MEKAL model.) As expected, the models differ in the character of their residuals over the Fe L region $\sim$0.7–1.2 keV. One effect of these differences is that the Raymond–Smith fits are not usually improved as much by letting $N_{\rm H}$ be a free parameter.

We also display in Table 4 the results for the absorbed cooling-flow model. For eleven galaxies the cooling-flow model with or without excess absorption fits the spectra with χ^2 values comparable to the MEKAL model. For the other nine galaxies (IC 1459 and 4296, NGC 1399, 1407, 4472, 4649, 5044, 5846 and 7626) the cooling-flow model fits the galaxy spectra better than the MEKAL model. In the cases of IC 4296, NGC 4472 and 5044 the improvement in the fits is dramatic (see Fig. 2). For the galaxies where allowing for excess absorption improved the fits to the MEKAL model, the fits with the cooling-flow model also improved with excess absorption and typically required a larger amount of absorption than did the MEKAL model.

The mass deposition rates of the cooling gas, $\dot{M}_{\rm gas}$, are mostly a few solar masses per year consistent with results from *Einstein* (Nulsen, Stewart & Fabian 1984; Thomas et al. 1986). We find generally good agreement with the mass deposition rates obtained from *ROSAT* studies for NGC 507 (Kim & Fabbiano 1995) and NGC 1399 (Rangarajan et al. 1995), although the Rangarajan et al. value of $\sim$1.7 $M_\odot$ yr^{-1} for NGC 1399 is about 50 per cent larger than our value. We find a larger value of $\dot{M}_{\rm gas}$ for NGC 4406 than Iwasawa et al. (1997) because our value refers to a larger extraction region.

For NGC 5044 we obtain a very large $\dot{M}_{\rm gas} \approx 75\,M_\odot$ yr^{-1} more appropriate for clusters of galaxies (e.g. Fabian 1994). A previous *ROSAT* study (David et al. 1994) of NGC 5044 found $\dot{M}_{\rm gas} \approx 20$–$25$ $M_\odot$ yr^{-1}. The larger value we obtain for NGC 5044 mostly occurs because of the large amount of excess absorption required by *ASCA* whereas for *ROSAT* the absorption is consistent with the Galactic value.

Interestingly, the abundances obtained from the cooling-flow models are generally much larger than those found from the regular MEKAL models. For the cooling-flow galaxies mentioned above the metallicities all have best-fiting values $Z \gtrsim 0.4\,Z_\odot$ except for IC 1459. If we consider all of the galaxies, the cooling-flow models give a mean and standard deviation, $\langle Z \rangle = 0.6 \pm 0.5\ Z_\odot$.

We mention that the larger values of $T_{\rm CF}$ with respect to those derived from the MEKAL model do not necessarily imply different gravitating masses. The value of $T_{\rm CF}$ is just the upper temperature from which the gas cools at constant pressure. The proper temperature to use for determining a virial mass is a (gas) mass-weighted

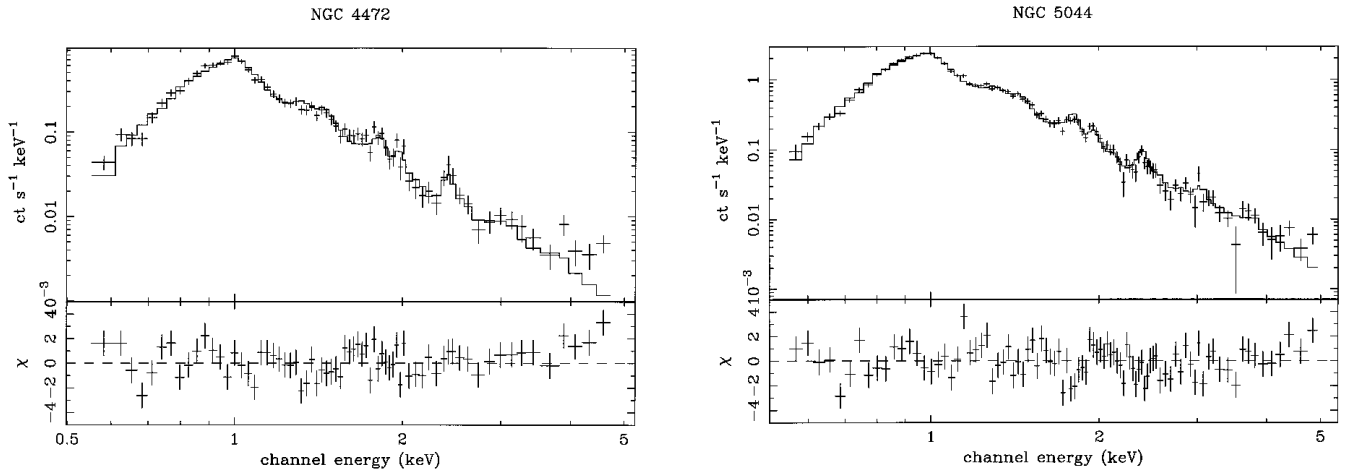

Figure 2. Fits of the absorbed cooling-flow model to NGC 4472 (left) and NGC 5044 (right). Only the SIS0 data is shown.

temperature. It should also be emphasized that there could exist complicated situations in a multiphase cooling flow where cold gas which has dropped out of the flow is supported by the hotter phases (e.g. via magnetic fields). Again, a (gas) mass-weighted temperature, or an appropriately adjusted mean molecular weight (which will be higher than the single-phase hot gas), must be used in the hydrostatic equation. This leads to a smaller gravitating mass than that inferred from the equation of hydrostatic equilibrium using $T_{\rm CF}$. These comments also apply to the two-temperature models discussed later (Section 3.2).

Interpretation of the fitted parameters for IC 1459 must be treated with caution. The high temperature, especially for the cooling-flow model, implies an implausibly large mass for an elliptical of its luminosity. Rather, emission from discrete sources with a likely contribution from a central AGN (owing to it being a radio source) suggest that emission from hot gas does not dominate the emission. This picture is consistent with the relatively small value of $L_{\rm x}/L_{\rm B}$ of IC 1459 and the results of two-temperature fits discussed in Section 3.2.

Finally, when jointly analysing the SIS+GIS data we obtained essentially the same answers as when analysing only the SIS data. However, some differences when analysing the GIS data alone deserve mention. First, for the high $L_{\rm x}/L_{\rm B}$ galaxies such as NGC 507 and NGC 4472, the required excess absorption depended sensitively on the lower energy bound used in the fits. For $\rm E_{low} = 0.8\,keV$ we obtained the best-fitting $N_{\rm H} = 0.01 \times 10^{21}$ cm^{-2} for NGC 507 and $N_{\rm H} = 2.3 \times 10^{21}$ cm^{-2} for NGC 4472 whereas for $\rm E_{low} = 1\,keV$ we obtained $N_{\rm H} = 1.8 \times 10^{21}$ cm^{-2} for NGC 507 and $N_{\rm H} = 1.6 \times 10^{21}$ cm^{-2} for NGC 4472; i.e. better agreement with the SIS data is seen for $\rm E_{low} = 1\,keV$. Secondly, for the low $L_{\rm x}/L_{\rm B}$ galaxies such as NGC 1332 and 3923 we find that the best-fitted temperatures are approximately 2 keV as opposed to about 0.6 keV with the SIS. These values are formally inconsistent within their errors and simply reflect the different energy resolutions and different effective areas as a function of energy of the SIS and GIS as discussed in Section 2.

3.1.2 Assessing the validity of measured abundances

The very subsolar abundances obtained from the single-temperature MEKAL and Raymond–Smith fits has cast doubt on the reliability of the plasma codes, in particular the accuracy to which the emission in the Fe L spectral region, 0.7−1.4 keV, is modelled (e.g. Arimoto et al. 1997). We have empirically tested the reliability of the MEKAL code by examining the behaviour of the fitted abundances and temperatures when the Fe L spectral region is excluded from the fits to the SIS data. This procedure is motivated by the fact that for gas with $T \sim 1$ keV the peak in the galaxy spectrum occurs in the Fe L region: the location of this peak is one measure of the temperature. Outside the Fe L region the continuum level provides an independent measure of the temperature. Comparing the temperatures (and abundances) determined inside and outside the Fe L region directly tests the consistency of the plasma code.

We analysed the restricted energy range, $E = 0.5-2$ keV, to limit the effects of a possible hotter component in the hot gas and/or a hard component arising from discrete sources. We fitted the MEKAL model with free $N_{\rm H}$ to the following two cases: (in) – the Fe L region and (out) – the energies excluding the Fe L region over 0.5–2 keV. For both (in) and (out) the initial parameters in the fits were specified by the model obtained from fitting the entire 0.5–2 keV range. For these fits we defined the Fe L region to be $E = 0.7-1.2$ keV. Although Fe L contributes up to energies ∼1.4 keV, the emission there is comparable to those from other elements (most notably Mg).

Let us suppose that the MEKAL model produces too much Fe L emission for a given T and Z.[3] The fits can suppress the excess Fe L emission by either increasing T or decreasing Z or both. Hence, in this case we would expect fits to region (in) to have higher T and/or smaller Z than fits to (out). We would expect the opposite behaviour if the MEKAL model produces too little Fe L emission for a given T and Z. (These arguments assume a single-temperature component dominates the emission over 0.5–2 keV.)

In Fig. 3 we plot temperatures and abundances for region (out) against those of region (in). For all but two galaxies (IC 1459 and 4296) the temperatures show little scatter along the line $T_{\rm in} = T_{\rm out}$ giving a strong indication of the validity of the MEKAL code in the Fe L region. The high inferred temperature of IC 1459 (see Table 4) accounts for its large value of $T_{\rm out}$ while the significant contribution from a higher temperature component over region (out) likely explains the position of IC 4296 (see Section 3.2).

The abundances show considerable scatter, but there appears to be an excess of galaxies above the line $Z_{\rm in} = Z_{\rm out}$; i.e. $Z_{\rm out}$ tends to exceed $Z_{\rm in}$ in our sample, although the effect is not large. Given the consistency of the temperatures, this excess $Z_{\rm out}$ may indicate that

[3] Relative abundances are fixed at their solar values.

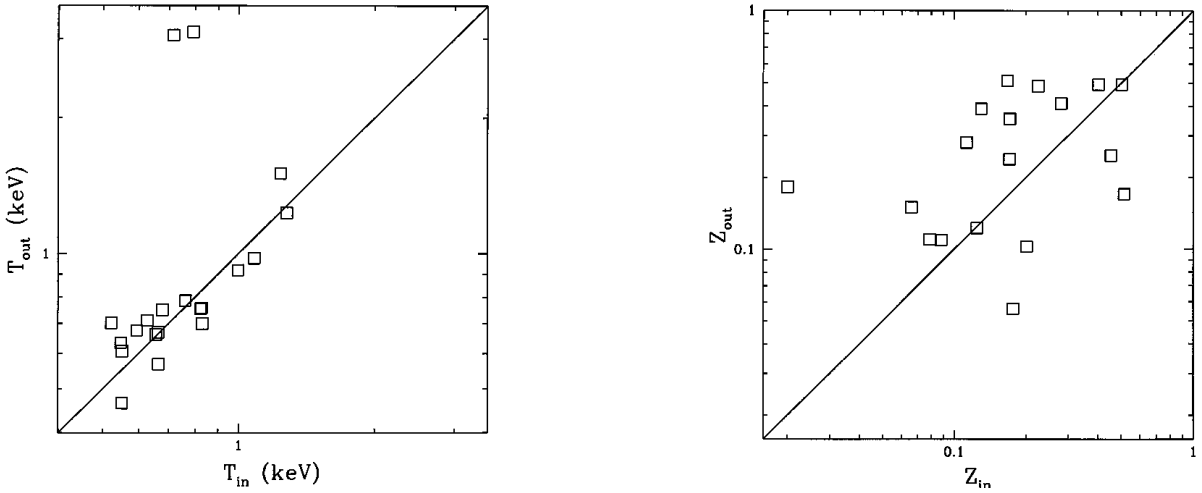

Figure 3. Empirical test of the reliability of the MEKAL code within the Fe L region. We show results of fitting an absorbed single-temperature MEKAL model to subdivisions of the energy range 0.5-2 keV. We designate the Fe L region (0.7-1.2 keV) as 'in' while the region over 0.5-2 keV excluding the Fe L region is designated as 'out'. The solid lines denote $T_{\rm in} = T_{\rm out}$ and $Z_{\rm in} = Z_{\rm out}$ respectively.

the abundances of the elements dominating the line emission of region (out) (i.e. Si) are slightly over-abundant with respect to Fe. Once again IC 1459 is the outlier (leftmost point).

Finally, in Fig. 4 we plot the ratio of temperature to abundance for region (out) versus region (in). If the Fe L emission of the MEKAL model is incorrect, then T/Z should tend to be larger in region (in) if MEKAL predicts too much Fe L emission or smaller if MEKAL predicts to little Fe L emission; i.e. the slope in the T/Z (in)–T/Z (out) plane will be negative if the MEKAL model incorrectly predicts the Fe L emission. However, no such trend is found in Fig. 4. Rather, T/Z for the regions tend to track each other, albeit with large scatter which is due mostly to the scatter in the abundances.

Hence, over 0.5–2 keV the MEKAL code gives very consistent results when applied to only the Fe L region (in) and to the region excluding the Fe L lines (out). The very subsolar abundances determined from the single-temperature fits of the MEKAL model are thus not the result of errors in the Fe L portion of the plasma code. As we show in the next section, these subsolar abundances arise from fitting a single-temperature model to an intrinsically multitemperature spectrum.

[We have performed the same tests using the Raymond–Smith model. The results are qualitatively similar to those found with the MEKAL model, although the scatter in the parameter relationships in regions (in) and (out) with the Raymond–Smith model is larger. Also $T_{\rm in}$ tends to exceed $T_{\rm out}$ for the Raymond–Smith model. Although the Raymond–Smith model, as expected, gives more evidence for problems in the Fe L regions than the MEKAL model, the differences do not appear to be huge. This is supported by the qualitative agreement that we obtained for the temperatures and abundances of the single-temperature MEKAL and Raymond–Smith models, although the higher temperatures and lower abundances of the Raymond–Smith model found in the previous section are consistent with over-prediction of the Fe L emission. As we discuss below, a large discrepancy between the MEKAL and Raymond–Smith models is not found for the two-temperature fits as well.]

3.2 Two-component fits

Since most of the single-temperature fits with the MEKAL model clearly provide unacceptable fits to the *ASCA* spectra, we examined whether the fits would improve significantly upon adding another temperature component. Our procedure is to begin with the best-fitted single-temperature model with Galactic $N_{\rm H}$ and then add another absorbed temperature component with $N_{\rm H}$ and Z tied to the first component. The normalization of the second component is initially set to zero. After fitting this two-temperature model we then allowed $N_{\rm H}$ to be free to see if the fit could be further improved.

The process of fitting these two component models to the *ASCA* spectra required some care to insure that the global χ^2 minimum was achieved by XSPEC for the galaxies having lowest S/N in our sample; i.e. for approximately half of the galaxies. Typically, upon initially fitting the two-temperature model to these lower S/N galaxies one finds that the first component, let us call it the cold component with temperature $T_{\rm C}$, has a best-fitting $T_{\rm C} \lesssim 1$ keV similar to that which was obtained with the single-temperature fits. The temperature of the second component, let us call it the hot component with temperature $T_{\rm H}$, typically has a best-fitting $T_{\rm H} \gtrsim 10$ keV. Also, the abundances tended to differ insignificantly from their single-temperature values.

We found, however, that for many of these galaxies these fits were not the global minima. By taking these best-fitting results and then initially setting $T_{\rm H}$ to some relatively small value (e.g.

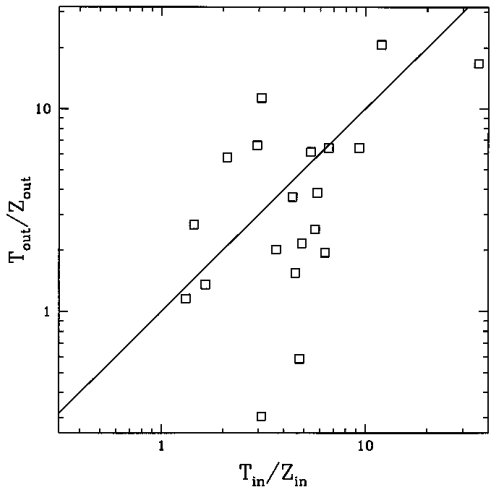

Figure 4. As Fig. 3 except that the ratios of temperature to abundance are plotted.

Table 5. Two-temperature bits.

Name	N_H (10^{21} cm^{-2})	T_C (keV)	T_H (keV)	Z ($Z_\odot$)	f_C/f_H (0.5-2 keV)	f_C/f_H (0.5-5 keV)	$\Delta\chi^2(N_H)$	χ^2	dof	χ^2_{red}
NGC 499	$2.0^{+0.4}_{-0.4}$	$0.65^{+0.03}_{-0.02}$	5.7(> 3.1)	$0.67^{+0.53}_{-0.24}$	11^{+7}_{-4}	$4.8^{+1.9}_{-1.2}$	32.2	231.9	200	1.16
NGC 507	$1.3^{+0.5}_{-0.5}$	$0.89^{+0.25}_{-0.22}$	$1.48^{+0.29}_{-0.17}$	$0.63^{+0.32}_{-0.20}$	$0.32^{+0.31}_{-0.23}$	$0.25^{+0.32}_{-0.18}$	10.4	60.8	72	0.85
NGC 720	...	$0.57^{+0.04}_{-0.05}$	7.4(> 3.6)	0.4(> 0.1)	$2.9^{+1.7}_{-0.9}$	$1.4^{+0.7}_{-0.3}$	...	42.6	45	0.95
NGC 1332	...	$0.54^{+0.04}_{-0.05}$	14(> 7)	0.8(> 0.2)	$2.22^{+0.78}_{-0.22}$	$0.96^{+0.39}_{-0.20}$	...	66.9	63	1.06
NGC 1399	$0.9^{+0.3}_{-0.3}$	$0.78^{+0.05}_{-0.05}$	$1.64^{+0.12}_{-0.09}$	$1.12^{+0.43}_{-0.23}$	$0.40^{+0.05}_{-0.03}$	$0.31^{+0.03}_{-0.03}$	28.8	310.9	251	1.24
NGC 1404	...	$0.60^{+0.02}_{-0.02}$	$2.13^{+0.92}_{-0.40}$	$0.7^{+2}_{-0.3}$	$3.9^{+1.2}_{-1.3}$	$2.7^{+1.1}_{-0.8}$	...	168.8	123	1.37
NGC 1407	...	$0.78^{+0.04}_{-0.04}$	3.9(> 2.9)	$0.53^{+0.98}_{-0.36}$	$1.59^{+2.35}_{-0.33}$	$0.87^{+0.90}_{-0.16}$	...	84.5	91	0.93
NGC 3923	...	$0.55^{+0.08}_{-0.13}$	4.2(> 2.2)	2.0(> 0.1)	$1.89^{+0.93}_{-0.62}$	$0.99^{+0.65}_{-0.23}$	...	21.8	20	1.09
NGC 4374	...	$0.66^{+0.05}_{-0.04}$	5.0(> 2.1)	$0.17^{+0.17}_{-0.09}$	$7.3^{+19}_{-3.9}$	$3.9^{+10}_{-1.8}$	...	59.3	49	1.21
NGC 4406	$1.0^{+0.4}_{-0.4}$	$0.70^{+0.03}_{-0.07}$	$1.22^{+0.30}_{-0.28}$	$0.52^{+0.22}_{-0.18}$	$2.9^{+1.7}_{-1.4}$	$2.4^{+1.2}_{-1.0}$	11.5	179.3	183	0.98
NGC 4472	$1.2^{+0.3}_{-0.3}$	$0.76^{+0.02}_{-0.03}$	$1.48^{+0.11}_{-0.09}$	$1.18^{+0.39}_{-0.26}$	$1.31^{+0.11}_{-0.08}$	$1.02^{+0.07}_{-0.06}$	56.6	260.0	235	1.11
NGC 4636	$1.2^{+0.3}_{-0.2}$	$0.65^{+0.02}_{-0.01}$	> 5.3	$0.35^{+0.08}_{-0.05}$	42^{+2}_{-8}	14^{+2}_{-3}	46.8	206.0	135	1.53
NGC 4649	$1.5^{+0.6}_{-0.5}$	$0.75^{+0.04}_{-0.04}$	$1.90^{+0.42}_{-0.26}$	$0.89^{+0.86}_{-0.29}$	$2.01^{+0.34}_{-0.19}$	$1.36^{+0.17}_{-0.10}$	21.0	131.8	96	1.37
NGC 5044	$1.5^{+0.2}_{-0.3}$	$0.70^{+0.02}_{-0.03}$	$1.20^{+0.05}_{-0.05}$	$0.62^{+0.11}_{-0.08}$	$0.85^{+0.09}_{-0.08}$	$0.72^{+0.08}_{-0.06}$	82.0	193.9	158	1.23
NGC 5846	$1.3^{+0.5}_{-0.4}$	$0.63^{+0.03}_{-0.04}$	$1.32^{+0.18}_{-0.21}$	$0.55^{+0.29}_{-0.19}$	$2.8^{+0.9}_{-0.7}$	$2.2^{+0.6}_{-0.4}$	13.6	92.8	104	0.89
NGC 6876	...	$0.90^{+0.14}_{-0.14}$	3.0(> 1.5)	$0.27^{+0.66}_{-0.17}$	$3.5^{+29}_{-2.4}$	$2.0^{+13}_{-1.1}$	...	21.0	16	1.31
NGC 7619	$3.4^{+1.0}_{-1.0}$	$0.65^{+0.05}_{-0.05}$	3.1(> 1.8)	1.2(> 0.3)	$9.3^{+16.1}_{-4.1}$	$4.3^{+3.5}_{-1.2}$	31.3	82.6	95	0.87
NGC 7626	...	$0.69^{+0.07}_{-0.06}$	$3.3^{+1.6}_{-1.0}$	2.0(> 0.4)	$1.6^{+0.6}_{-0.4}$	$1.1^{+0.2}_{-0.4}$	...	52.8	49	1.08
IC 1459	...	$0.66^{+0.09}_{-0.10}$	$7.8^{+16}_{-3.0}$	$0.14^{+0.67}_{-0.09}$	$0.36^{+0.67}_{-0.01}$	$0.22^{+0.26}_{-0.03}$	...	58.9	52	1.13
IC 4296	...	$0.75^{+0.05}_{-0.04}$	$5.0^{+1.3}_{-1.2}$	2.8(> 0.9)	$0.94^{+0.47}_{-0.13}$	$0.49^{+0.32}_{-0.05}$	...	86.7	88	0.99

Results of fitting 2 MEKAL models each modified by the same photoelectric absorption. If allowing N_H to be free significantly improved the fit, we give the best-fitting value of N_H and the change in χ^2 denoted by $\Delta\chi^2(N_H)$. The '...' indicate that letting N_H be free did not significantly improve the fits. The abundances, Z, are tied together in the fits. The best-fitting values and their 90 per cent confidence limits on one interesting parameter are given. f_C/f_H is the flux of the absorbed cold component divided by that of the absorbed hot component.

1−2 keV) and the abundances to some relatively large value $Z \sim (1-2)Z_\odot$ and then fitting again we found that a deeper minimum was usually obtained. The results of this new deeper minimum were generally smaller values of T_H and larger values of Z, although in most cases the 90 per cent confidence regions overlapped with those of the previous minimum.

For example, the initial fit for IC 4296 yielded ($T_C = 0.81$ keV, $T_H = 18.4$ keV, $Z = 0.20\,Z_\odot$, $\chi^2 = 93.8$). By then resetting T_H and Z to small and large values respectively, we obtained (after performing this procedure twice) best-fitting values ($T_C = 0.75$ keV, $T_H = 5.0$ keV, $Z = 2.8\,Z_\odot$, $\chi^2 = 86.7$) as given in Table 5: the change in χ^2 is greater than 2.71. The other galaxies showed a smaller effect. Initial fits to NGC 720 gave ($T_C = 0.57$ keV, $T_H = 41.4$ keV, $Z = 0.18\,Z_\odot$, $\chi^2 = 43.7$). The results listed in Table 5 show that the change in χ^2 is only 1.1, but the best-fitting parameters and their confidence regions (although overlapping) are qualitatively different; i.e. the abundance in the deeper minimum is unbounded from above unlike that in the shallower minimum.

In Table 5 we list the results of fitting two absorbed MEKAL models to each galaxy in the sample. In Fig. 5 we plot the two-temperature fits corresponding to the same galaxies in Fig. 1. In all but a few cases the improvement in the fits is substantial and the values of reduced χ^2 are brought to approximately 1.0. (We found that untying the abundances and/or absorption of the components did not significantly improve the fits.)

As expected, the galaxies like NGC 507, 4374 and 4406, which already had reduced $\chi^2 \approx 1.0$ from fits to a single MEKAL model, generally showed the smallest improvement when another component was added. For NGC 1404 the poor fit is mostly because of residuals near 1.8 keV in the observation sequence 80039000. The origin of these residuals is unclear (they are not seen in the spectrum of NGC 1399 from the same sequence), but if we exclude this sequence we obtain a reduced $\chi^2 \sim 1$ for the single-temperature model and thus, like NGC 507, 4374 and 4406, a single temperature appears to produce the emission without great (formal) need for another component.

For NGC 6876, which has the poorest S/N of the sample, letting N_H be free substantially improved the fit, $\chi^2 \approx 16.5$, but the resulting fitted parameters were very poorly constrained. (Because of the low S/N we were unable to obtain a definite best-fitting result because the χ^2 space contained many small isolated minima of similar depth.) The 90 per cent confidence regions, however, include the parameter space obtained when N_H is held at the Galactic value, and thus we have presented those results in Table 5.

As expected (see Section 2), when fitting the SIS+GIS data we found, as with the single-temperature fits of the previous section, that the results differed negligibly from the SIS results alone. We shall henceforth focus on the SIS results.

3.2.1 *Temperatures*

The effect of adding the second temperature component can be divided roughly into two classes. For the galaxies with the best S/N and typically the largest L_x/L_B the two temperature components essentially bracket the single-temperature value with $T_C \sim 0.5-1$ keV and $T_H \sim 1-2$ keV. These temperatures are consistent with emission from hot gas. For the galaxies having large S/N and large L_x/L_B but $T_H > 2$ keV (NGC 499, 4636 and 7619), the cold component dominates the X-ray emission. Hence, the high S/N, high L_x/L_B galaxies either have no evidence for emission from a hard component with $T_H \gtrsim 5$ keV or allow for only a small fraction ($\lesssim$10 per cent) of the total flux to reside in such a component. Rather, multiple phases in the hot gas are indicated by the two-temperature (and three-temperature, see below) fits. The fits to most of these galaxies are also significantly improved by allowing for excess absorption. In Section 4 we discuss in detail the evidence and implications for this excess absorbing material. (We reiterate that the fits are not significantly improved by allowing for individually

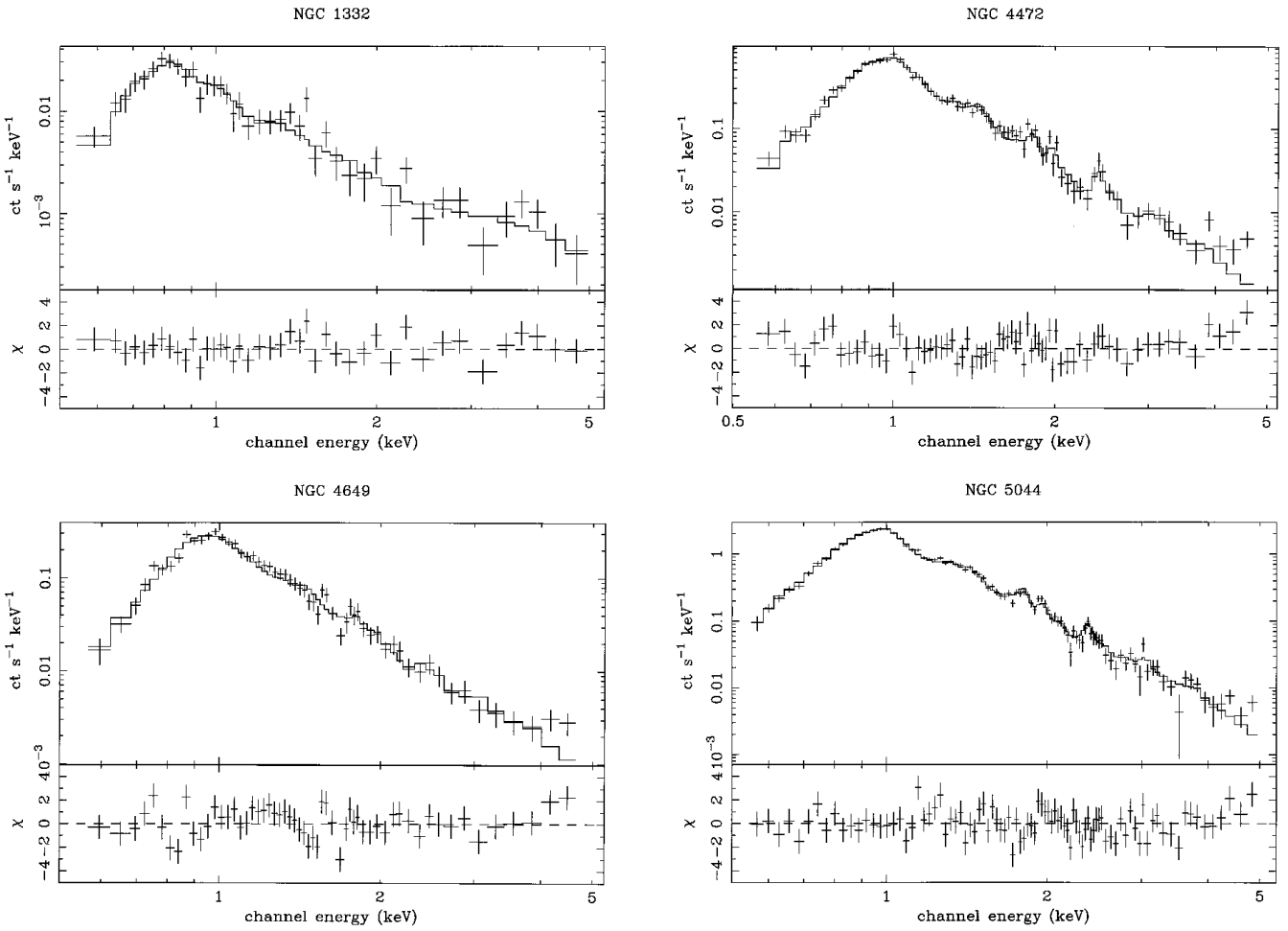

Figure 5. As Fig. 1 but the spectra are fit with absorbed two-temperature (MEKAL) models.

fitted abundances for the cold and hot components, or by letting the α-process elements be fitted separately from Fe.)

The other galaxies, those with lowest S/N and smallest L_x/L_B, typically have $T_C \sim 0.5-1$ keV (similar to the single-temperature value) and $T_H \sim 5-10$ keV. The cold component is consistent with emission from hot gas while the hotter component has temperatures consistent with that expected from discrete sources (e.g. Kim et al. 1992); i.e. this putative discrete component is found to be most important in galaxies that tend to have the lowest L_x/L_B ratios in our sample as expected (Canizares et al. 1987). Typically the emission from the cold component exceeds that of the hot component in the soft energy range, 0.5–2 keV, while the emission from each component is roughly equal over the full 0.5–5 keV band. IC 1459 is the exception as its hot component dominates, which again suggests that its emission is qualitatively different from others in our sample and may indicate the emission from the AGN.

For the galaxies with $T_H \sim 3-5$ keV having large L_x/L_B but average S/N in our sample, it is possible that higher S/N data will split T_H into another soft component and a hard component. (This may even happen for the lowest L_x/L_B galaxies.) Interpretation of the nature of the hotter component in these galaxies must await better quality data.

NGC 4636 has the worst formal fit of the galaxies in our sample that does not have any obvious anomalous features in its spectrum (see Fig. 6). Untying the absorptions and abundances of the components did not improve the fits. We tried grouping the α-process elements (O, Ne, Mg, Si and S) separately from Fe and the rest to no avail. The best improvement in χ^2 was obtained by adding a third temperature component (see Table 6 and Fig. 6).

The fit was not improved greatly and so there may be something special to NGC 4636 inhibiting a good fit. A new 200-ks observation of NGC 4636 shows the same anomalous spectrum indicating that the features are real and not the result of a spurious observation (Buote et al. in preparation). The addition of the third temperature component split T_C into two roughly equal components with temperatures between 0.5 and 1 keV. The flux of the high-temperature component remains dwarfed by the soft components. The substantial residuals for $E < 1$ keV and the fact that NGC 4636 has a low value of T_C for its X-ray luminosity (see Fig. 9 in Section 3.2.4) suggests the presence of additional cold phases.

Essentially all of the other galaxies are not affected significantly by adding another temperature component, although NGC 4472 and especially NGC 4649 show some improvement (see Table 6). In these two cases the added component has a temperature with no upper bound and may indicate the emission from discrete sources in those galaxies. Again, the softer components dominate the hard component.

Fitting two Raymond–Smith models to the galaxy spectra gives χ^2 values that are qualitatively similar to those obtained from the MEKAL models in many cases, but there are notable differences. Generally, the reduced χ^2 values of the Raymond–Smith fits are

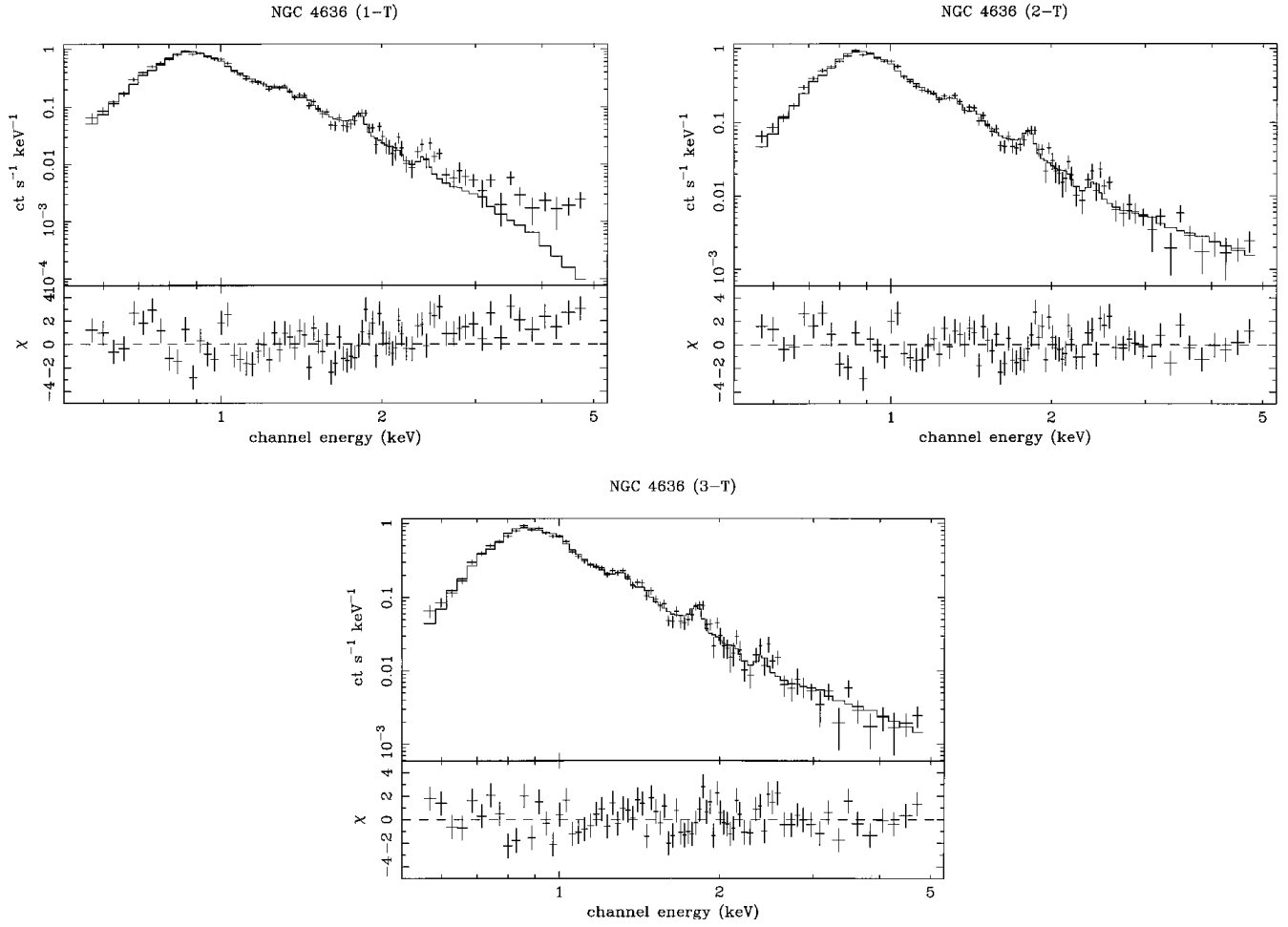

Figure 6. Single-temperature (1-T), two-temperature (2-T), and three-temperature (3-T) (MEKAL) models fit to NGC 4636. Only the SIS0 data is shown.

larger, $(\chi^2_{\rm red})^{\rm RS} \sim (\chi^2_{\rm red})^{\rm MEKAL} + 0.2$. However, the fits to NGC 1399 ($\chi^2_{\rm red} = 1.43$) and NGC 4472 ($\chi^2_{\rm red} = 1.47$) are noticeably poorer than the MEKAL fits while NGC 4636 ($\chi^2_{\rm red} = 2.65$) and NGC 4472 ($\chi^2_{\rm red} = 1.96$) have dramatically worse fits. These galaxies coincidentally have the best S/N (and among the largest $L_{\rm x}/L_{\rm B}$) in the sample.

When $N_{\rm H}$ was allowed to be free the fits with the Raymond–Smith model were not improved as much as were fits with the MEKAL model. Only NGC 507, 4649, 5044, 6876 and 7619 showed significant improvement but with a lesser change in χ^2 than found with the MEKAL model.

The fits to the galaxies using the Raymond–Smith code also gave qualitatively comparable temperatures to those determined with MEKAL, although both $T_{\rm C}$ and $T_{\rm H}$ tend to be larger for Raymond–Smith.[4] Typically, $T_{\rm C}^{\rm RS} \sim T_{\rm C}^{\rm MEKAL} + 0.2$. For galaxies where $T_{\rm H} \sim 5$ keV as determined from the MEKAL model, the Raymond–Smith fits tend to give $T_{\rm H} > 10$ keV; for many of these only lower limits could be found. We found that the Raymond–Smith fits gave $T_{\rm H} < 2$ keV for only NGC 1404, 4472, 5044 and 5846. Interestingly, when $N_{\rm H}$ is allowed to be free for NGC 4472 the best-fitting value of $T_{\rm H}$ increases without bound, although the quality of the fit is not significantly improved. (The abundances in these two cases are quite different as we mention below.) Hence, the nature of the emission of the second temperature component, be it due to another phase of the hot gas or to discrete sources, is dependent on the plasma code; i.e. MEKAL tends to give smaller $T_{\rm H}$ and thus more indication of additional phases of the hot gas than Raymond–Smith.

10 of the galaxies in our sample have been previously analysed by Matsumoto et al. (1997) using *ASCA* data (see Section 1). These authors fit a two-component model to the SIS and GIS spectra where each component is modified by the same variable absorption, and the abundances of each component are tied together. For IC 1459 and 4296, NGC 499, 720, 4374 and 4636, where we found $T_{\rm C} \sim 0.5-1$ keV and $T_{\rm H} \gtrsim 5$ keV, Matsumoto et al. obtained $T_{\rm C}$ and reduced χ^2 values (and $N_{\rm H}$) in good agreement with our results – whether we used two MEKAL models or Raymond–Smith models. (We have different reduced χ^2 values for NGC 507 because we excluded its anomalous SIS1 data – see the beginning of Section 3.) For NGC 4406, 4472 and 4649 Matsumoto et al. obtained comparable quality fits to us without requiring a second hot phase. As mentioned above, this is as a result of fitting Raymond–Smith models instead of MEKAL models.

We also obtained essentially the same $T_{\rm C}$ and $T_{\rm H}$ of Buote & Canizares (1997) who fitted two Raymond–Smith components to NGC 720 and 1332. The unbounded $T_{\rm H}$ (and low abundance) obtained by Buote & Canizares using two Raymond–Smith models agrees with our findings using the same models. Our Raymond–Smith fits for NGC 4374, 4406, 4472 and 4636 give $T_{\rm C}$ and $T_{\rm H}$ in good agreement with the results of Matsushita et al.

[4]This is consistent with the Raymond-Smith model predicting too much Fe L emission for a particular T and Z – see Section 3.1.2.

Table 6. Three-temperature fits.

Name	$N_{\rm H}$ (10^{-21} cm^{-2})	T_1 (keV)	T_2 (keV)	T_3 (keV)	Z ($Z_\odot$)	$f_1 : f_2 : f_3$ (0.5-2 keV)	(0.5-5 keV)	χ^2	dof	$\chi^2_{\rm red}$
NGC 4472	$1.3^{+0.3}_{-0.3}$	$0.73^{+0.03}_{-0.03}$	$1.34^{+0.10}_{-0.08}$	> 6	$1.19^{+0.46}_{-0.28}$	21 : 17 : 1	7.0 : 7.1 : 1	246.4	230	1.07
NGC 4636	$1.4^{+0.5}_{-0.4}$	$0.53^{+0.10}_{-0.17}$	$0.73^{+0.20}_{-0.07}$	8(> 3)	$0.47^{+0.17}_{-0.12}$	15 : 12 : 1	6.1 : 5.0 : 1	181.7	132	1.38
NGC 4649	$2.0^{+0.9}_{-0.7}$	$0.67^{+0.07}_{-0.08}$	$1.15^{+0.21}_{-0.22}$	> 5	$0.88^{+0.41}_{-0.33}$	9.7 : 7.3 : 1	3.1 : 2.7 : 1	110.0	93	1.18

Results of fitting three MEKAL models each modified by the same photoelectric absorption for three galaxies where the fit is at least marginally improved. The abundances, Z, are tied together in the fits. The best-fitting values and their 90 per cent confidence limits on one interesting parameter are given for the column densities, temperatures and abundances. The best-fitting ratio of the fluxes of component 1 to component 3 and the ratio of component 2 to component 3 are given by $f_1 : f_2 : f_3$.

(1994) who fitted two Raymond–Smith components to the GIS data.

Our results for NGC 5044 appear to be consistent with those from Fukazawa et al. (1996) who fitted single-temperature models to *ASCA* SIS and GIS data in the regions $R < 2$ arcmin and 4 arcmin $< R <$ 6 arcmin and found $\chi^2_{\rm red} > 1.42$ for a suite of four plasma codes. Since the residuals of the fit of their single-temperature Raymond–Smith model (see their fig. 4) are very consistent with our findings (e.g. with the MEKAL model in Fig. 1), a two-temperature model with both temperatures lower than 2 keV would appear to be required for an acceptable fit to their spectra.

3.2.2 *Abundances*

The metal abundances obtained from the two-temperature (and three-temperature) MEKAL models are substantially larger than those obtained from the single-temperature models. For 18 out of 20 galaxies we find that the best-fitting metal abundances for the two-temperature models have $Z > 0.4\,Z_\odot$. The mean and standard deviation of the abundances for the entire sample are $\langle Z\rangle = 0.9 \pm 0.7\ Z_\odot$. The two galaxies (IC 1459 and NGC 4374) having very subsolar abundances also have among the lowest S/N spectra in our sample.[5]

This systematic increase of Z derived for the two-temperature models with respect to single-temperature models occurs because of an intrinsic bias specific to X-ray spectral fitting. As noted in Section 2.2 of Buote & Canizares (1994) regarding the analysis of the *ROSAT* PSPC spectrum of NGC 720 with the Raymond–Smith code, when a galaxy spectrum which is intrinsically described by a two-temperature solar abundance model is fitted with a single-temperature model, the fitted abundance will necessarily have a value that is very subsolar; i.e. the very subsolar abundances are an artificial systematic bias of fitting single-temperature models to intrinsically multitemperature spectra. We verified this result using simulated two-temperature *ASCA* spectra with MEKAL models for the highest S/N galaxies in our present sample.[6] (We mention that for the galaxies where excess absorption improved the fits, when the absorption is fixed to its Galactic value the abundances are usually about the same as for the fits allowing for excess absorption, though in some cases the abundances are considerably larger; e.g. for NGC 4649 we obtain $Z = 0.89\,Z_\odot$ when allowing for excess absorption but $Z = 1.24\,Z_\odot$ for Galactic $N_{\rm H}$. Thus the relatively large abundances are not the result of the (in some cases) large required $N_{\rm H}$ suppressing the excess line emission at lower energies.)

Hence, the very subsolar abundances obtained by previous studies with *ROSAT* (e.g. Davis & White 1996) and *ASCA* (e.g. Arimoto et al. 1997) which fitted single-temperature models to the X-ray spectra of ellipticals appear to be a fitting artifact. However, even recent studies with *ASCA* which fitted two-temperature models obtained typical abundances that are significantly less than solar. For example, Matsushita et al. (1994) analysed a small sample of early-type galaxies and obtained $Z \approx 0.4\,Z_\odot$ for NGC 4406, 4472, and 4636, and $Z \approx 0.1\,Z_\odot$ for NGC 4374 by fitting two Raymond–Smith components to GIS data. Our Raymond–Smith results produce similar values except for NGC 4472 where we obtain $Z = 1.3\,Z_\odot$. We obtain qualitatively similar results for these galaxies with fits to two MEKAL models. If we let $N_{\rm H}$ be free for the fit to NGC 4472 with two Raymond–Smith models, then we obtain $Z = 0.5\,Z_\odot$ in much better agreement with Matsushita et al. (although the fit is not improved significantly).

These four galaxies, however, have somewhat smaller abundances than our entire sample. For the fits with two Raymond–Smith models we obtain for the whole sample an abundance with mean and standard deviation, $\langle Z\rangle = 0.7 \pm 0.6\ Z_\odot$. This value is systematically smaller than obtained from the fits with two MEKAL models, but the relatively small systematic difference is consistent with our findings in Section 3.1.2.

However, these abundances are still systematically larger than the abundances ($Z \lesssim 0.4\,Z_\odot$) obtained by Matsumoto et al. (1997) who analyzed a sample of 12 early-type galaxies (see Section 1). The disagreement with our results probably is because of the different modelling procedures. That is, although Matsumoto et al. use a variable temperature Raymond–Smith model for their soft component, they use a fixed, 12 keV, bremsstrahlung temperature for the hard component. (And they let $N_{\rm H}$ be free in all cases, regardless of whether the fit demands that it be different from the Galactic values.) We explained near the beginning of Section 3.2 that larger values of $T_{\rm H}$ tend to imply smaller values of Z, especially for the galaxies having spectra with the lowest S/N. Considering that Matsumoto et al. generally use larger extraction apertures than us (particularly for the SIS1) their spectra have lower S/N and thus these effects become more pronounced.

Thus, the modelling differences and lower S/N data likely account for the differences between our present study and those of Matsumoto et al. (The updated *ASCA* calibration used in our paper also contributes to these differences.) Since the MEKAL model is more accurate than Raymond–Smith, and we believe there is no reason to bias the fits with a preconceived hard component required to be present in the same form in all galaxies, and our data have

[5] We note that it would be better to quote a mean abundance weighted by the uncertainties in the individual measurements. However, the error bars are highly asymmetric and the sizes of the errors are highly correlated with the measured value of Z. Thus, a simple weighting by standard errors is inappropriate.

[6] Some *ROSAT* studies cautioned that poor quality spectra simply could not distinguish between single-temperature models with very subsolar abundances and two-temperature models with solar abundances (e.g. Trinchieri et al. 1994) owing to the larger number of free parameters in the latter case.

Table 7. Intrinsic (unabsorbed) luminosities of the cold component (L_x^C) and the hot component (L_x^H) in erg s^{-1} corresponding to the two-temperature models of Table 5. We used the distances from Faber et al. (1989) as reported in Eskridge, Fabbiano & Kim (1995) for $H_0 = 50$ km s^{-1} Mpc^{-1}.

Name	$\log_{10} L_x^C$		$\log_{10} L_x^H$		$\log_{10} L_x/L_B$	
	(0.5-2 keV)	(0.5-5 keV)	(0.5-2 keV)	(0.5-5 keV)	(0.5-2 keV)	(0.5-5 keV)
NGC 499	42.55	42.57	41.39	41.70	−1.16	−1.12
NGC 507	42.19	42.21	42.66	42.76	−1.40	−1.32
NGC 720	40.76	40.77	40.30	40.58	−2.58	−2.48
NGC 1332	40.43	40.44	40.07	40.43	−2.70	−2.55
NGC 1399	41.30	41.32	41.66	41.77	−1.65	−1.56
NGC 1404	41.23	41.24	40.64	40.80	−2.02	−1.97
NGC 1407	40.97	40.99	40.75	41.01	−2.43	−2.31
NGC 3923	40.89	40.90	40.58	40.83	−2.76	−2.65
NGC 4374	41.04	41.06	40.17	40.45	−2.57	−2.51
NGC 4406	41.78	41.79	41.29	41.37	−1.86	−1.83
NGC 4472	41.59	41.61	41.43	41.54	−2.22	−2.17
NGC 4636	41.97	41.98	40.28	40.69	−1.60	−1.58
NGC 4649	41.41	41.42	41.06	41.20	−2.26	−2.20
NGC 5044	42.80	42.81	42.82	42.89	−0.64	−0.60
NGC 5846	41.96	41.97	41.46	41.54	−1.69	−1.66
NGC 6876	41.51	41.55	41.00	41.23	−2.03	−1.94
NGC 7619	42.25	42.26	41.09	41.31	−1.51	−1.49
NGC 7626	41.06	41.07	40.82	41.05	−2.44	−2.34
IC 1459	40.47	40.49	40.71	41.03	−2.62	−2.39
IC 4296	41.53	42.00	41.54	41.81	−2.29	−1.90

generally higher S/N, the approximately solar abundances found in this paper would appear to be favoured. Possible abundance gradients do not resolve our discrepancy with previous studies because we obtain approximately solar abundances even for some of the large S/N galaxies in our sample which have large extraction radii (e.g. NGC 1399 and 4472). Approximately solar abundances are consistent with multiphase models for the evolution of the hot gas in ellipticals (e.g. Fujita, Fukumoto & Okoshi 1997) but are still inconsistent with the highly supersolar abundances predicted by standard enrichment models (e.g. Ciotti et al. 1991; also see Arimoto et al. 1997).

3.2.3 *Cooling flows*

We also fitted the galaxy spectra to a two-component model consisting of a cooling-flow model for one component and a MEKAL model for the other. The absorption and abundances were handled as with the two MEKAL models above. In all cases we found that these models gave fits of essentially the same quality as obtained with the two MEKAL models. Generally, the fitted temperatures and abundances behaved similarly as well. For galaxies with both temperature components less than about 2 keV the MEKAL component can be thought to represent either the ambient gas phase or the gravitational work done on the flow, and the cooling-flow component the distributed mass drop-out term. It should be emphasized that T_{CF} is the maximum temperature from which the gas cools (i.e. not the emission-weighted temperature).

For example, we found for NGC 5044 the temperature of the cooling-flow component to be, $T_{CF} = 1.6$ keV, that of the MEKAL component to be, $T_M = 0.94$ keV, and the abundance to be $Z = 0.94\,Z_\odot$; as with the single-temperature fits, the abundances obtained with cooling-flow models are larger. The flux of the cooling-flow component is dominant, $f_{CF}/f_M = 3.6$ (0.5–2 keV). The inferred mass deposition rate, $\dot{M}_{gas} = 47\,M_\odot$ yr^{-1}, is less than that obtained in the single-component case since the flux is now shared with the other component.

3.2.4 *Luminosities*

In Table 7 we give the unabsorbed luminosities of the cold and hot components obtained from the fits of the two MEKAL models to the galaxy spectra as well as the ratio of total X-ray luminosity, $L_x = L_x^C + L_x^H$, to L_B. (We give only the best-fitting values of L_x since the statistical uncertainties are less than a few per cent. The statistical errors on the relative contribution of L_x^C and L_x^H are very nearly those of f_C/f_H in Table 5.) Because of our procedure of maximizing the S/N of the extraction radii (Section 2) our luminosities tend to be somewhat smaller than found in previous studies which is most significant for galaxies having the lowest S/N observations. However, the 0.5–5 keV fluxes determined in this paper differ by $\lesssim$25 per cent for the corresponding galaxies studied by other authors using larger aperture sizes (Awaki et al. 1994; Matsushita et al. 1994; Loewenstein et al. 1994; Buote & Canizares 1997; Arimoto et al. 1997; Matsumoto et al. 1997), and thus the luminosities in Table 7 are close to the total values.

We plot the total X-ray luminosity versus L_B in Fig. 7. As expected for the relatively high L_x/L_B galaxies in our sample (Canizares et al. 1987), the slope is quite steep, $d \ln L_x / d \ln L_B \sim 2$, and is consistent with that predicted from steady-state cooling flow models (Nulsen et al. 1984; Sarazin 1997). Although our sample is too small to make a definitive statement, the slope appears to steepen for larger L_x and L_B. These galaxies include NGC 1399, 5044 and 5846 for which significant emission may be as a result of a diffuse intergroup medium.

Also in Fig. 7 we plot the emission from the soft and hard components separately. We take the emission of the soft components to be given by those of the cold component with temperature T_C. If $T_H < 2$ keV then we add that emission to the soft component as well. The hard components are those having $T_H \gtrsim 5$ keV. The slope of the soft emission appears to be slightly steeper than that of the total X-ray emission for the galaxies with smaller L_x. We can not distinguish the slopes of the soft and hard components (although the

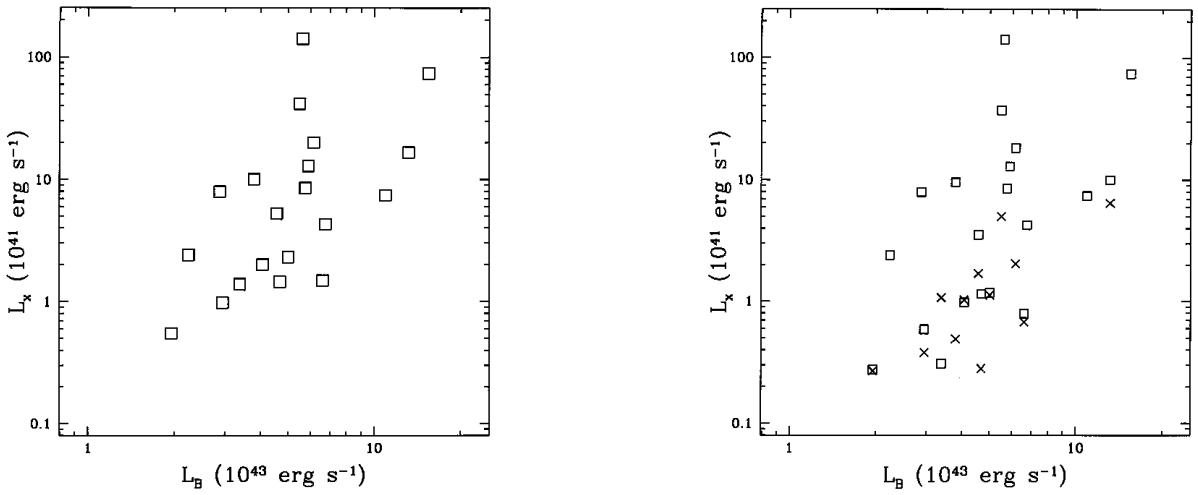

Figure 7. (left) The total 0.5–5 keV band X-ray luminosity versus L_B and (right) 0.5–5 keV band luminosities of the cold components (boxes) and hard components (crosses).

galaxies with measured hard components do not extend to the highest L_x in our sample), but the hard component does appear to flatten somewhat at the largest L_B.

In any event, the slope for the hard emission is still considerably steeper than 1 which indicates for the galaxies in our sample the hard components are not entirely associated with discrete sources. It is likely that with higher S/N data the temperatures of many of these hard components will be split into subcomponents some of which will have smaller temperatures consistent with emission from hot gas.

As argued in previous studies of large samples of ellipticals with the *Einstein Observatory* (Canizares et al. 1987; Kim et al. 1992) the ratio L_x/L_B is a good indicator of when the X-ray emission is dominated by hot gas (larger values) or by discrete sources (smaller values). In Fig. 8 we plot the ratio of the luminosity of the cold component to the hot component, L_x^C/L_x^H, versus L_x/L_B. Galaxies which have $T_H < 2$ keV are not plotted since they have no measured component presumably owing to discrete sources, but would appear somewhere in the top right of the plot. We see an increase of L_x^C/L_x^H with L_x/L_B as expected, albeit with large scatter, and a slope slightly less than 1. Hence, from direct measurement of the ratio L_x^C/L_x^H we have shown that as L_x/L_B increases the proportion of the total emission because of hot gas with respect to that of a hard component presumably as a result of discrete sources increases such that $\mathrm{d}\ln(L_x^C/L_x^H)/\mathrm{d}\ln(L_x/L_B) \sim 1$. Interestingly, for a general slope α this relation implies that when $L_x^C/L_B \rightarrow \infty$ we have $L_x^H \rightarrow L_B/\alpha^2$ which is consistent with expectations of a discrete component where $L_x^{disc} \propto L_B$.

Finally, we plot the temperature of the soft component versus total X-ray luminosity in Fig. 9. This temperature is taken to be T_C unless $T_H < 2$ keV in which case it is set to the emission-weighted value of T_C and T_H. Over the decade in luminosity $L_x = (0.5-5)\times 10^{41}$ erg cm^{-2} s^{-1} we see the expected rise of temperature of the hot gas with total X-ray luminosity. However, the trend disappears into scatter for larger L_x. For example, NGC 7619 and NGC 7626 have low T_C for their X-ray luminosity. However, they also have $T_H \sim 3$ keV and thus their hot-gas temperatures may in fact be higher in reality.

Another explanation is given by cooling flows. We infer mass deposition rates of $\dot{M}_{gas} > 1\,M_\odot$ yr^{-1} for galaxies NGC 499, 4636, 7619, 7626 and IC 4296 which appear to have low soft temperatures for their X-ray luminosity. Hence, as in clusters of galaxies (Fabian et al. 1994), the presence of cooling flows may account for much of the scatter in the L_x-T_x relationship.

4 THE EVIDENCE FOR EXCESS ABSORPTION AND ITS IMPLICATIONS

For approximately half the galaxies in our sample the spectral fits are significantly improved when allowing for absorption in excess of the Galactic value. This effect is most clearly illustrated for the galaxies where the cooling-flow model provides a substantially better fit than a single MEKAL (or Raymond–Smith) model (see Section 3.1). In Fig. 10 we display the SIS0 spectrum of NGC 1399 and the best-fit cooling-flow model obtained from jointly fitting the SIS0 and SIS1 data of the two available observations (see Table 1). When fixing N_H to the Galactic value the best-fitting model predicts more emission than observed for energies $\sim$0.6–0.8 keV: $\chi^2 = 575.0$ for 257 dof giving $\chi^2_{red} = 2.24$. These residuals around 0.8 keV cannot be eliminated by including another thermal

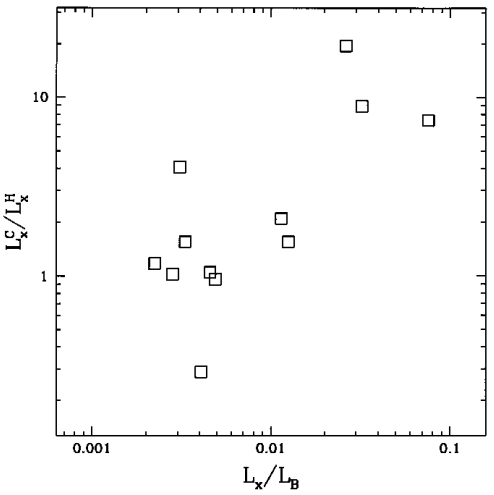

Figure 8. The ratio of L_x^C (the luminosity of the cold component) to L_x^H (the luminosity of the hot component) versus L_x/L_B, where $L_x = L_x^C + L_x^H$. Only galaxies with $T_H > \sim 5$ keV are plotted, while those with $T_H < \sim 2$ keV (indicating another hot gas phase) would appear somewhere in the upper right corner of the figure. All luminosities are evaluated in the 0.5–5 keV band.

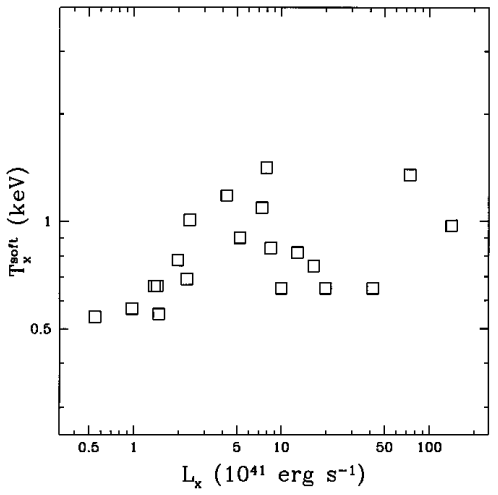

Figure 9. The temperature of the soft component versus the 0.5–5 keV total X-ray luminosity. The soft temperature is equal to T_C for galaxies with $T_H > \sim 5$ keV and is the emission weighted value of T_C and T_H for galaxies where $T_H < \sim 5$ keV.

component. However, if the absorbing column is allowed to be a free parameter then these residuals can be largely removed: $\chi^2 = 341.3$ for 256 dof giving $\chi^2_{red} = 1.33$. The resulting column density, $N_H = 1.8^{+0.3}_{-0.2} \times 10^{21}$ cm^{-2}, is over 10 times the Galactic value of $N_H = 0.13 \times 10^{21}$ cm^{-2} (Stark et al. 1992).

Is this excess absorption an instrumental effect peculiar to *ASCA*? As explained in Section 3.1, most previous *ROSAT* studies do not find evidence for excess absorption in early-type galaxies. This discrepancy between the spectral shape of *ROSAT* and *ASCA* below 1 keV has been observed, e.g. for the bright Seyfert galaxies MCG-6-30-15 (Nandra & Pounds 1992) and NGC 5548 (Iwasawa et al., in preparation) as well as the classic QSO 3C273 (Yaqoob et al. 1994). However, a recent analysis of MCG-6-30-15 by Orr et al. (1997a) finds that the $\sim 0.1 - 10$ keV spectrum observed by *Beppo-SAX* (Parmar et al. 1997) agrees extremely well with that of the *ASCA* SIS. Similar agreement between *Beppo-SAX* and *ASCA* has also been reported for 3C273 (Orr et al. 1997b). Furthermore, from a simultaneous *ROSAT* PSPC and ASCA observation of the Seyfert galaxy NGC 5548 (Iwasawa et al., in preparation) it has been found that the absorption determined from *ASCA* agrees with determinations from *Ginga* unlike the determination from *ROSAT*. Given the agreement between the spectra of *ASCA*, *SAX*, and *Ginga* it would appear that the excess absorption measured by *ASCA* is not the result of an instrumental effect.

We do note that the excess column density reported here, if resulting from a uniform screen of the galaxy, precludes any emission being detected in the carbon band of *ROSAT*. Of course, the excess absorption is likely to be distributed throughout the emitting gas, and the nearest unabsorbed parts of the galaxy will give detectable radiation in that band. (See Allen & Fabian 1997 for simulations of this effect for clusters of galaxies.)

We mention that Rangarajan et al. (1995) did find excess absorption for NGC 1399 by exploiting the spatial information provided by the *ROSAT* PSPC. By comparing the ratios of the spectrum of the inner region ($r \lesssim 10$ kpc) to a best-fitting unabsorbed thermal model with the corresponding ratio of the spectrum of an outer annulus ($r \sim 100-150$ kpc) to its best-fitting unabsorbed thermal model they clearly showed the diminution of photons with energies $\lesssim 1$ keV in the inner region (see their fig. 5). However, consistent with the general *ASCA–ROSAT* discrepancy stated above, excess absorption is not required when fitting absorbed (single-component) thermal models to the data (Jones et al. 1997).

The excess N_H we have derived from the spectral fits is only the simplest result assuming a uniform absorber that reduces the X-ray emission according to an exponential form depending only on the energy. In this approximation the excess columns $N_H \approx (1-3) \times 10^{21}$ cm^{-2} imply masses in atomic hydrogen, $M_{abs} \approx 5 \times 10^9 M_\odot$, when spread uniformly over a 10 kpc radius. This level of absorber mass is very similar to the typical mass of the hot X-ray emitting gas in early-type galaxies, but M_{abs} is typically a factor of 10 larger than the mass inferred from H I observations (e.g. Bregman, Roberts & Giovanelli 1988; Bregman & Roberts 1990). Similar disagreement is found for an absorption feature in the field of NGC 4472 by Irwin & Sarazin (1996). However, these discrepancies with H I observations may be irrelevant since the absorber could be composed of molecular gas (e.g. Ferland, Fabian & Johnstone 1994). The mass of molecular gas can be measured with CO observations, but is typically factors of a few smaller than expected under the above simple assumptions (e.g. Irwin, Frayer & Sarazin 1997). However, excess absorbing mass above that predicted by the standard CO/H_2 conversion has been reported from

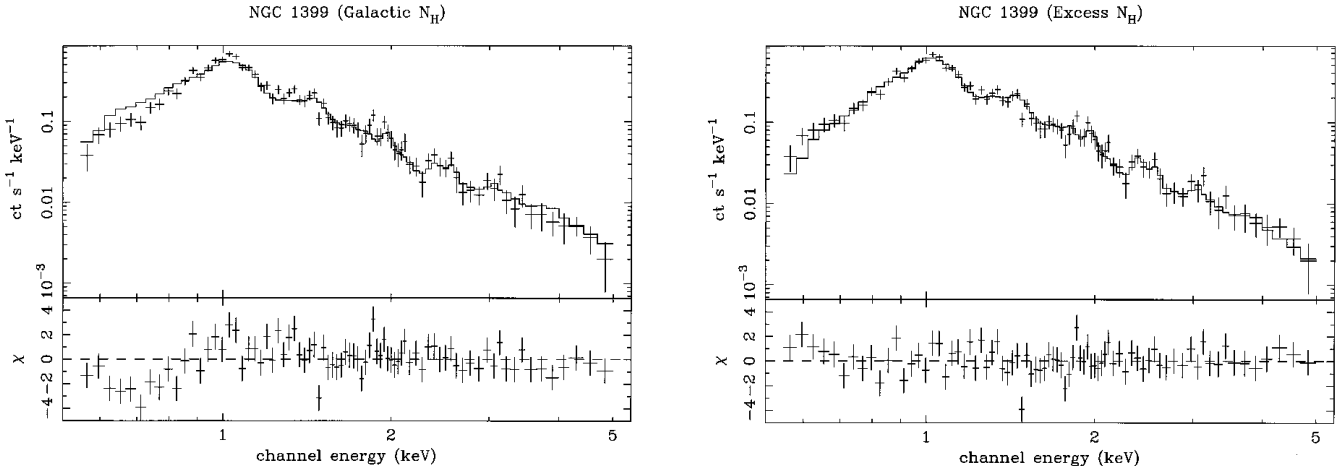

Figure 10. Fits of the absorbed cooling-flow model to NGC 1399 with fixed Galactic absorption (left) and with variable absorption (right). Only the SIS0 data is shown for sequence 80038000.

158- μm observations of the irregular galaxy IC 10 (Madden et. al 1997). It should be emphasized that the uniform absorber model is certainly over-simplified and, e.g. a partial covering fraction and metallicity dependence could very well be required.

The cold gas implied by the excess absorption is a natural consequence of the multiphase cooling-flow scenario (Nulsen 1986; Thomas et al. 1987; White & Sarazin 1987) wherein mass drops out of the flow at all radii where the cooling time is less than the age of the galaxy ($t_{\rm age}$). In particular, for clusters of galaxies Allen & Fabian (1997) have demonstrated using color profiles of *ROSAT* PSPC data that clusters with $t_{\rm cool} \ll t_{\rm age}$ have intrinsic absorbing material which is preferentially distributed in the core and of a quantity that is consistent with the amount of mass deposited by the cooling flow over $t_{\rm age}$.

Although the situation in early-type galaxies is likely complicated to some extent by heat sources, the success of the simple cooling-flow model over the single MEKAL model for the brightest galaxies and the associated required excess absorption (see Section 3.1) suggests that multiphase cooling flows are operating in these galaxies. This is further supported by the fact that these galaxies when fitted with two-temperatures indicate that they have a multiphase medium (see Section 3.2); i.e. one component may represent the hot ambient phase and the other the emission from the distributed mass drop-out component. In this scenario, the drop-out term should consist of a continuum of phases which will become evident when probed by detectors with better spectral resolution.

5 CONCLUSIONS

We present spectral analysis of *ASCA* data of 20 bright, mostly high $L_{\rm x}/L_{\rm B}$, early-type galaxies (17 E, three S0) which is the largest sample of its kind reported to date. Fitting a single, absorbed, thin thermal model (MEKAL or Raymond–Smith) to the spectra fails to provide acceptable fits (e.g. $\chi^2_{\rm red} > 1.5$) for 14 galaxies. Excess absorption significantly improves the fits for 10 of the galaxies. The abundances of the single-temperature models are very subsolar, $\langle Z\rangle = 0.19 \pm 0.12\ {\rm Z}_\odot$, in agreement with those reported by previous *ROSAT* and *ASCA* studies.

Fitting instead an absorbed cooling-flow model yields fits of comparable quality to the MEKAL model for 11 galaxies but is a significantly better fit for the other nine. The improvement in the fits is dramatic for NGC 4472, 5044 and IC 4296. The abundances obtained from the cooling-flow model, $\langle Z\rangle = 0.6 \pm 0.5\ {\rm Z}_\odot$, significantly exceed those obtained with the MEKAL and Raymond–Smith models.

We empirically tested the reliability of the MEKAL and Raymond–Smith plasma codes in the Fe L band. In order to lessen the influence of other temperature components we restricted our analysis to 0.5–2 keV and performed fits over only the Fe L band (taken to be 0.7–1.2 keV) and over the band excluding Fe L (0.5–0.7 and 1.2–2 keV). We did not find large systematic trends expected if the plasma codes predict too much or too little Fe L emission for a given temperature and metallicity. However, unlike the MEKAL model, the Raymond–Smith model did give some evidence for these systematic trends which, as expected, indicates that the Fe L region of Raymond–Smith is not as well modeled as with MEKAL. (The reasonable agreement of the abundances obtained by MEKAL and Raymond–Smith shows that such errors are not catastrophic.)

Fitting two-temperature models (with MEKAL or Raymond–Smith models) significantly improved the quality of the fit in 16 out of 20 galaxies and gave formally acceptable values of $\chi^2_{\rm red} \sim 1.0$. (We found that care needed to be exercised with XSPEC to achieve the global χ^2 minima for the lowest S/N galaxies in the sample.) The galaxies having the highest S/N spectra in our sample (which coincidentally have the largest $L_{\rm x}/L_{\rm B}$) generally have a temperature for the cold component, $T_{\rm C} \sim 0.5-1$ keV, and for the hot component, $T_{\rm H} \sim 1-2$ keV; i.e. both components are consistent with emission from hot gas.[7] The lower S/N galaxies (which coincidentally have the smallest $L_{\rm x}/L_{\rm B}$) typically have $T_{\rm C} \sim 0.5-1$ keV but $T_{\rm H} \gtrsim 5$ keV. The temperature of this hot component is consistent with emission from discrete sources. The flux of this hot component is generally smaller than that of the cold component.

In stark contrast to the single-temperature models, the abundances obtained from the two-temperature fits are approximately solar; $\langle Z\rangle = 0.9 \pm 0.7\,{\rm Z}_\odot$ for two MEKAL models and $\langle Z\rangle = 0.7 \pm 0.6\ {\rm Z}_\odot$ for two Raymond–Smith models. The difference between the abundances determined from single-temperature and two-temperature models is not because of increased errors on the parameters but is an artefact of fitting intrinsically multitemperature spectra with single-temperature models (Buote & Canizares 1994).

Our abundances disagree with the two-component models fit to *ASCA* spectra of several of the galaxies in our sample by Matsumoto et al. (1997). We attribute the discrepancy to the different modeling procedures used and to the higher S/N data in our study owing to generally smaller extraction radii for the spectra. Possible abundance gradients do not account for the discrepancy because we obtain approximately solar abundances even for some of the large S/N galaxies in our sample which have large extraction radii (e.g. NGC 1399 and 4472). The approximately solar abundances we find are consistent with multiphase models for the evolution of the hot gas in ellipticals (e.g. Fujita et al. 1997). However, though considerably larger than obtained in previous studies, these nearly solar abundances are still substantially less than the super-solar abundances predicted by the standard enrichment theories (e.g. Ciotti et al. 1991; also see Arimoto et al. 1997).

Two-component models where one component is a cooling-flow model and the other a MEKAL give fits of comparable quality to fits of two MEKAL models. Since the flux is shared by the two components, the inferred mass deposition rates are smaller than when only a cooling-flow model is fitted to the spectra.

It should be emphasized that a radial temperature gradient in a single-phase gas unlikely accounts for the temperatures seen in the large $L_{\rm x}/L_{\rm B}$ galaxies. For example, NGC 4472 has roughly an equal contribution from phases with temperatures $T_{\rm C} = 0.76$ keV and $T_{\rm H} = 1.48$ keV, but the temperature profile measured with the *ROSAT* PSPC varies from only $\sim$0.75–1.1 keV over $r \leq 4$ arcmin (Irwin & Sarazin 1996). A plausible physical explanation of the two phases is offered by a multiphase cooling flow (Nulsen 1986; Thomas et al. 1987; White & Sarazin 1987) where one component represents the hot ambient phase and the other represents the

[7] Recently Loewenstein & Mushotzky (1997) claim that ratios of the H-like to He-like Si lines in, e.g. NGC 1399 are only consistent with an isothermal gas with temperature near 1 keV and inconsistent with the multiphase solution we find in Section 3.2. We have examined such line ratios and find that the line ratios of the single-temperature models in Secion 3.1 are very similar to those of the two-temperature models in Section 3.2 (i.e. within $\sim$15 per cent). However, caution must be exercised when computing these line ratios directly from the data because of the calibration errors owing to the optical constants in the mirror around 2 keV (Gendreau & Yaqoob 1997). Since the key H-like Si line appears at 2.0 keV, and for all of the galaxies in our sample this line is very noisy (e.g. Fig. 10), and its intensity depends sensitively on the assumed continuum, we believe that any reliable constraints on the 2.0 keV H-like Si line must await corrected response matrices.

emission from the distributed mass drop-out component. In this scenario, the drop-out term should consist of a continuum of phases which should become evident when probed by detectors with better spectral resolution.

We compared L_B to the luminosities of the hot and cold components determined by fits of two MEKAL models. Both the luminosities of the soft and of the hard components increase with L_B with a slope of approximately 2, although there is some weak evidence that the cold component has a steeper slope than the hot component. For galaxies with $T_H \gtrsim 5$ keV we find that $L_x^C/L_x^H \sim L_x/L_B$; i.e. there is a clear increase in the ratio of the luminosity of the cold component to the hot component as a function of L_x/L_B indicating that L_x/L_B is indeed a good indicator for the relative contribution of hot gas and discrete sources to the total X-ray emission. (A recent study of NGC 3923 by Buote & Canizares (1998) finds that the allowed contribution to the *ROSAT* X-ray emission from a population of discrete sources with $L_x \propto L_{optical}$ is significantly less than indicated by L_x^C/L_x^H measured in this paper if we associate $L_x^H \propto L_{optical}$. This would support the conjecture that a significant fraction of the hard components measured for the low S/N galaxies is due to other phases in the hot gas.)

Therefore, our investigation shows that the very subsolar abundances obtained in previous studies are not the result of failures in the plasma codes (as proposed by Arimoto et al. 1997). Rather, fitting multi-temperature models, without restricting the form of the models to a universal model for discrete sources, and setting extraction radii so that S/N is maximized, gives metal abundances near solar for both MEKAL and Raymond–Smith models.

Moreover, fits to the X-ray spectra of half of the galaxies in our sample are significantly improved when allowing for absorption in excess of the Galactic value. Accurate determination of the spatial distributions of the absorbing components and the various phases of the hot gas must await better quality data as must determination of the nature of the hard components found in the lower S/N galaxies in our sample. The next generation of X-ray satellites soon to be flown will have the capabilities to make significant progress in these areas.

ACKNOWLEDGMENTS

We acknowledge helpful discussions with S. Allen and K. Iwasawa on the reduction of *ASCA* data and K. Gendreau on *ASCA* calibration. This research has made use of (1) *ASCA* data obtained from the High Energy Astrophysics Science Archive Research Center (HEASARC), provided by NASA's Goddard Space Flight Center and (2) the NASA/IPAC Extragalactic Database (NED) which is operated by the Jet Propulsion Laboratory, California Institute of Technology, under contract with the National Aeronautics and Space Administration.

REFERENCES

Allen S. W., Fabian A. C., 1997, MNRAS, 286, 583
Anders E., Grevesse N., 1989, Geochimica et Cosmochimica Acta, 53, 197
Arimoto N., Matsushita K., Ishimaru Y., Ohashi T., Renzini A., 1997, ApJ, 477, 128
Arnaud K., 1996, in Jacoby G., Barnes J., eds, ASP Conf. Ser. Vol. 101, Astronomical Data Analysis Software and Systems V. Astron. Soc. Pac., San Francisco, p. 17
ASCA Guest Observer Facility, The *ASCA* Data Reduction Guide. Laboratory for High Energy Astrophysics, Greenbelt, MD, NASA/GSFC
Awaki H. et al., 1994, PASJ, 46, L65
Balucińska-Church M., McCammon D., 1992, ApJ, 400, 699
Bregman J. N., Roberts S., 1990, ApJ, 362, 828
Bregman J. N., Roberts S., Giovanelli R., 1988, ApJ, 330, L93
Buote D. A., Canizares C. R., 1994, ApJ, 427, 86
Buote D. A., Canizares C. R., 1997, ApJ, 474, 650
Buote D. A., Canizares C. R., 1998, MNRAS, in press (astro-ph/9803208)
Canizares C. R., Fabbiano G., Trinchieri G., 1987, ApJ, 312, 503
Ciotti L., D'Ercole A., Pellegrini S., Renzini A., 1991, ApJ, 376, 380
Dalle Ore C., Faber S. M., Jesús J., Stoughton R., 1991, ApJ, 366, 38
David L. P., Jones C., Forman W., Daines S., 1994, ApJ, 428, 544
Davis D. S., White R. E., III, 1996, ApJ, 470, L35
de Vaucouleurs G., de Vaucouleurs A., Corwin H.G., Buta R. J., Paturel G., Fouqué P., 1991, Third Reference Catalogue of Bright Galaxies. Univ. Texas Press, Austin (RC3)
Eskridge P. B., Fabbiano G., Kim D.-W., 1995, ApJS, 97, 141
Fabbiano G., Kim D.-W., Trinchieri G., 1992, ApJS, 80, 531
Faber S. M., Wegner G., Burstein D., Davies R. L., Dressler A., Lynden-Bell D., Terlevich R. J., 1989, ApJS, 69, 763
Fabian A. C., 1994, ARA&A, 32, 277
Fabian A. C., Crawford C. S., Edge A. C., Mushotzky R. F., 1994, MNRAS, 267, 779
Ferland G. J., Fabian A. C., Johnstone R. M., 1994, MNRAS, 266, 399
Forman W., Jones C., Tucker W., ApJ, 1985, 293, 102
Forman W., Schwarz J., Jones C., Liller W., Fabian, A. 1979, ApJ, 234, L27
Forman W., Jones C., David L., Franx M., Makishima K., Ohashi T., 1993, ApJ, 418, L55
Fujita Y., Fukumoto J., Okoshi K., 1997, ApJ, 488, 585
Fukazawa Y. et al., 1996, PASJ, 48, 395
Garcia A. M., 1993, A&AS, 100, 47
Gendreau K., Yaqoob T., 1997, *ASCA* XRT Calibration Issues, in *ASCA* News vol. 5. NASA/GSFC, Greenbelt, MD
Idesawa E. et al., 1997, Calibration of Temporal and Spatial Variations of the GIS Gain, ftp://legacy.gsfc.nasa.gov/asca/gisinformation/gain.ps/gz
Irwin J. A., Sarazin C. L., 1996, ApJ, 471, 683
Irwin J. A., Frayer D. T., Sarazin C. L., 1997, in Soker N., ed., ASP Conf. Ser. Vol. 115, Galactic and Cluster Cooling Flows. Astron. Soc. Pac., San Francisco, p. 75
Ishisaki Y. et al., 1997, Reproducibility of the GIS Non–X-Ray Background, in *ASCA* News vol. 5. NASA/GSFC, Greenbelt, MD
Iwasawa K., White D. A., Fabian A. C., 1997, MNRAS, submitted
Johnstone R. M., Fabian A. C., Edge A. C., Thomas P. A., 1992, MNRAS, 255, 431
Jones C., Stern C., Forman W., Breen J., David L., Tucker W., Franx M., 1997, ApJ, 482, 143
Kaastra J. S., Mewe R., 1993, A&AS, 97, 443
Kim D.-W., Fabbiano G., 1995, ApJ, 441, 182
Kim D.-W., Fabbiano G., Trinchieri G., 1992, ApJ, 393, 134
Liedahl D. A., Osterheld A. L., Goldstein W. H., 1995, ApJ, 438, L115
Loewenstein M., Mathews W. G., 1991, ApJ, 373, 445
Loewenstein M., Mushotzky R. F., 1997, Proc. IAU Symp. 187, Cosmic Chemical Evolution. in press (astro-ph/9710339)
Loewenstein M. et al., 1994, ApJ, 436, L75
Madden S. C., Poglitsch A., Geis N., Stacey G. J., Townes C. H., 1997, ApJ, 483, 200
Matsumoto H., Koyama K., Awaki H., Tsuru T., Loewenstein M., Matsushita K., 1997, ApJ, 482, 133
Matsushita K. et al., 1994, 436, L41
Mewe R., Gronenschild E. H. B. M., van den Oord G. H. J., 1985, A&AS, 62, 197
Nandra K., Pounds K. A., 1992, Nat, 359, 215
Nulsen P. E. J., 1986, MNRAS, 221, 377
Nulsen P. E. J., Stewart G. C., Fabian A. C., 1984, MNRAS, 208, 185
Orr A., Molendi S., Fiore F., Grandi P., Parmar A. N., Owens A., 1997a, A&A, in press (astro-ph/9706133)
Orr A. et al., 1997b, in The Active X-Ray Sky: Results from *Beppo-SAX* and *Rossi XTE*, held 21–24 October in Rome
Parmar A. et al., 1997, A&AS, 122, 309
Rangarajan F. V. N., Fabian A. C., Forman W. R., Jones C., 1995, MNRAS, 272, 665

Raymond J. C., Smith B. W., 1977, ApJS, 35, 419
Sarazin C. L., 1997, in Arnaboldi M., Da Costa G. S., Saha P., eds, Proc. Second Stromlo Symp. The Nature of Elliptical Galaxies. in press
Stark A. A., Gammie C. F., Wilson R. W., Bally J., Linke R. A., Heiles C., Hurwitz M. 1992, ApJS, 79, 77
Tanaka Y., Inoue H., Holt S. S., 1994, PASJ, 46, L37
Thomas P. A., Fabian A. C., Arnaud K. A., Forman W., Jones C., 1986, MNRAS, 222, 655
Thomas P. A., Fabian A. C., Nulsen P. E. J., 1987, MNRAS, 228, 973
Trinchieri G., Fabbiano G., Kim D.-W., 1996, A&A, 318, 361
Trinchieri G., Kim D.-W., Fabbiano G., Canizares C., 1994, ApJ, 428, 555
White D. A., Fabian A. C., Johnstone R. M., Mushotzky R. F., Arnaud K. A., 1991, MNRAS, 252, 72
White R. E., III, Sarazin C. L., 1987, ApJ, 318, 621
Yaqoob T. et al., 1994, PASJ, 46, L49

This paper has been typeset from a TEX/LATEX file prepared by the author.